UNIVERSITY OF PORTSMOUTH

US AFSOR Study Report

The effects of LCF loadings on HCF crack growth

Annual Report for Phase 1

F565

April 1998

Submitted by:

R. F. Hall and B.E.Powell

28 April 1998

MECHANICAL BEHAVIOUR OF MATERIALS LABORATORY

DEPARTMENT OF MECHANICAL AND MANUFACTURING ENGINEERING
Anglesea Building, Anglesea Road
Portsmouth PO1 3DJ
Phone: +44 (0)1705 842324/5 Fax: +44 (0)1705 842351
E-mail bpowell@mech.port.ac.uk

REPORT DOCUMENTATION PAGE

Form Approved OMB No. 0704-0188

1. AGENCY USE ONLY (Leave blank)	2. REPORT DATE	3. REPORT TYPE AND DATES COVERED
	28 April 1998	Final Report

4. TITLE AND SUBTITLE

The Effects of LCF Loading on HCF Crack Growth

5. FUNDING NUMBERS

F6170897W0112

6. AUTHOR(S)

R.F. Hall & B.E. Powell

7. PERFORMING ORGANIZATION NAME(S) AND ADDRESS(ES)

University of Portsmouth
Anglesea Building
Anglesea Road
Portsmouth PO1 3DJ
United Kingdom

8. PERFORMING ORGANIZATION REPORT NUMBER

N/A

9. SPONSORING/MONITORING AGENCY NAME(S) AND ADDRESS(ES)

EOARD
PSC 802 BOX 14
FPO 09499-0200

10. SPONSORING/MONITORING AGENCY REPORT NUMBER

SPC 97-4021

11. SUPPLEMENTARY NOTES

12a. DISTRIBUTION/AVAILABILITY STATEMENT

Approved for public release; distribution is unlimited.

12b. DISTRIBUTION CODE

A

13. ABSTRACT (Maximum 200 words)

This report results from a contract tasking University of Portsmouth as follows: The contractor will investigate the effects of low-cycle fatigue (LCF) on high-cycle fatigue (HCF) crack growth for aerospace propulsion applications.

14. SUBJECT TERMS

Structural Dynamics, Structures, Structural Materials

15. NUMBER OF PAGES

42

16. PRICE CODE

N/A

17. SECURITY CLASSIFICATION OF REPORT	18. SECURITY CLASSIFICATION OF THIS PAGE	19, SECURITY CLASSIFICATION OF ABSTRACT	20. LIMITATION OF ABSTRACT
UNCLASSIFIED	UNCLASSIFIED	UNCLASSIFIED	UL

UNIVERSITY OF PORTSMOUTH

US AFSOR Study Report

The effects of LCF loadings on HCF crack growth

Annual Report for Phase 1

F565

April 1998

Submitted by:

R. F. Hall and B.E.Powell

28 April 1998

MECHANICAL BEHAVIOUR OF MATERIALS LABORATORY

DEPARTMENT OF MECHANICAL AND MANUFACTURING ENGINEERING
Anglesea Building, Anglesea Road
Portsmouth PO1 3DJ
Phone: +44 (0)1705 842324/5 Fax: +44 (0)1705 842351
E-mail bpowell@mech.port.ac.uk

The effect of LCF loadings on HCF crack growth

Report for the period 28 April 1997- 27 April 1998

Report No F 565

Submitted by R. F. Hall and B. E. Powell

Notation

CN	=	corner notched
CT	=	compact tension
HCF	=	high cycle fatigue
LCF	=	low cycle fatigue
da/dN_{HCF}	=	crack growth increment resulting from the application of a HCF cycle
da/dN_{LCF}	=	crack growth increment resulting from the application of a LCF cycle
da/dB	=	crack growth increment resulting from the application of a HCF / LCF loading block
da/dB_{HCF}	=	crack growth increment resulting from the application of the HCF cycles within a loading block
da/dB_{LCF}	=	crack growth increment resulting from the application of the LCF cycles within a loading block
ΔK	=	stress intensity range
ΔK_{HCF}	=	stress intensity range associated with a HCF cycle
ΔK_{LCF}	=	stress intensity range associated with a LCF cycle, i.e. the peak-to-peak load cycle
ΔK_{onset}	=	the value of ΔK_{LCF} associated with the onset of HCF crack growth
ΔK_{th}	=	threshold value of stress intensity range
$K_{max,th}$	=	threshold value of maximum stress intensity
N_{HCF}	=	number of HCF cycles in a loading block
N_{LCF}	=	number of LCF cycles in a loading block
n	=	ratio $N_{HCF} : N_{LCF}$
R_{HCF}	=	stress ratio of the HCF cycles
R_{LCF}	=	stress ratio of the LCF cycles

1. Introduction

The design of critical rotating aero-engine components, and the demonstration of their structural integrity, must include an assessment of their fatigue lives in the presence of significant levels of vibration. In such components a low cycle fatigue (LCF) loading arises from the large cyclic variation of the conjoint centrifugal and thermal stresses. In the

simplest case this large stress variation occurs once per flight. However, rotating engine components have also experienced high cycle fatigue (HCF) failures as a direct result of vibrations of small amplitude. When they occur, these high frequency vibrations will be superimposed on part of each flight cycle. Consequently the fatigue integrity assessment requires an evaluation of the behaviour of aero-engine materials under the conjoint action of LCF and HCF loadings. Furthermore, it is essential that there is confidence in both the life prediction method used in such an assessment and the fatigue and fracture mechanics data it requires.

1.1 Fatigue Crack Growth

Powell et al [**1**] have shown that the fatigue crack growth curve for a loading combining HCF/LCF cycles in a fixed proportion is characterised by two regimes of behaviour (Figure **1**). These regimes are evident in the double logarithmic plot of the growth increment per HCF/LCF loading block (da/dB) versus the peak-to-peak range of stress intensity which gives rise to LCF (ΔK_{LCF}). At the lower values of ΔK_{LCF} (regime 1) the range of stress intensity associated with the HCF cycles is below a threshold value, and the individual HCF cycles do not contribute to the advance of the crack. As a consequence, the growth rates and fractographic appearance correspond to those for a LCF loading only. At the higher values of ΔK_{LCF} (regime 2) the range of stress intensity associated with the HCF cycles exceeds the threshold, and each HCF cycle now contributes to the growth. This contribution may cause the growth rate to increase rapidly, so deviating from the response due to the application of a separate LCF loading. The fracture surface may now exhibit "block striations", that is to say, striation markings generated by each peak-to-peak cycle which are well-separated by regions of growth due to the HCF cycles [**2-4**]. The value of ΔK_{LCF} corresponding to the transition between these two regimes is labelled ΔK_{onset}.

The simplest model for the prediction of fatigue crack growth rates due to combined HCF/LCF loadings assumes that there are no effects due to load history or load sequence. Thus the linear summation model adds the growth increments due to the LCF stress cycle and all the HCF cycles, to give the growth rate for the combined HCF/LCF loading block (da/dB). Powell et al [**3, 5**] have shown examples where the linear summation rule has been

successful, and where, due to load interactions or short crack effects, it has not. In order to accommodate load interaction effects, Hawkyard et al [**6**] have analysed the fatigue threshold values and near-threshold growth rates associated with the HCF cycles by ascribing all the potential load history effects to the HCF cycle component of the loading. Satisfactory crack propagation life predictions were achieved for a wide range of HCF/LCF loadings applied to forged Ti-6Al-4V at room temperature by combining this approach with a model based on the concept of crack closure. A similar result was obtained by Claridge and Powell [**7**] using a commercial software package whose algorithm for crack life predictions also employs the concept of crack closure in modelling the fatigue behaviour of materials. Significantly, Evans et al [**8**] have used closure corrected data to successfully predict the crack growth response of IMI 829 at 350°C for a range of HCF/LCF loadings.

If the vibrational stresses are of sufficient number and amplitude, a significant reduction in the fatigue crack growth life is observed, with the transition between the two growth rate regimes marking, for all practical purposes, the effective end of the crack growth life. Comparisons between the HCF threshold value associated with this transition and the threshold value determined in constant amplitude load shedding tests, have been made in a range of materials [**9-12**]. Both agreements and discrepancies have been observed. In the latter case, attempts have been made to correlate the HCF threshold value at the transition with the threshold value determined by a method involving a step change in stress ratio (the "jump - in" method). In this way improved correlations have been achieved, but more often they have not. In order to clearly understand this important aspect of material behaviour, a systematic study of threshold values, derived from the transition between the two growth rate regimes, load shedding tests, and jump-in experiments, is required.

Fundamental studies into the effects of the conjoint action of HCF/LCF stress cycles inevitably use tests which involve a substantial simplification of the LCF cycle generated in service. In practice different stress levels will be developed in critical components during the various stages of each flight. Recent unpublished work conducted at the University of Portsmouth, has examined the growth of cracks during a flight sequence in which vibrational loads were superimposed during the simulated stages of take-off, climb and

cruise. This work highlighted the need to account for the load history effects when assessing the contribution to the overall growth from the HCF cycles. In particular it was necessary to characterise the crack growth due to superimposed HCF cycles when preceded by an overload.

1.2 Scope of the report

This report describes three aspects of the present study. First, the re-analysis of the results of past studies on the effect of HCF and LCF loadings, both when applied separately and in combination, on the fatigue crack growth rate behaviour of forged Ti-6Al-4V. Second, is the presentation of the predicted fatigue crack growth rates for combined LCF/HCF loading experiments involving systematic variations in the ratio of HCF to LCF cycles within each repeated loading block. The analysis allows for overloads within the LCF loading and considers the effect of their magnitude. Third, is a description of the development of the test facility able to apply a wide range of HCF/LCF loadings, achieved through the modification of the HCF/LCF isolation unit and the installation of new load control and test monitoring systems.

2. Re-analysis of data for Forged Ti-6Al-4V

Forged Ti-6Al-4V is extensively used by all aero-engine manufacturers for critical rotating components. As a consequence, this material was used in the earliest experiments conducted at the University of Portsmouth into the fatigue crack growth behaviour of aero-engine alloys under HCF and LCF loadings. Inevitably, and rightly, the data obtained formed a base-line against which the responses of more creep resistant alloys were subsequently compared. In the light of the renewed interest in the effects of HCF and LCF loadings, the present need is to extend both the data-base for forged Ti-6Al-4V and the understanding of its behaviour. Thus, it is appropriate to first reassess the data that has been obtained and used for this purpose in the past [**3, 6, 9, 13-15**].

Compact tension (CT) and corner notched (CN) specimens of forged Ti-6Al-4V were cut from unused fan and compressor discs. The applied loads used in their testing consisted of:

1. HCF cycles with a stress ratio of 0.7-0.95 and a frequency of 150 Hz,
2. LCF cycles having a trapezoidal waveform, a stress ratio of 0.1,
3. Combinations of HCF and LCF cycles in which the HCF cycles were restricted to the dwell period at the maximum load of the LCF cycles.

Full details of the test material, procedures and data analysis have been reported elsewhere **[3, 6, 9, 13-15]**.

2.1 HCF thresholds and crack growth rates

The previously obtained experimental data relating to threshold values for Ti-6Al-4V forged material has been reviewed, re-analysed and collated. Thus, Figures **2** and **3** contain the accumulated threshold data, including that which was derived from tests combining HCF with LCF using a process (called back calculation) which partitioned the overall crack growth rates into that due to the HCF and the LCF loading components **[16]**. The effect of stress ratio on the threshold value is shown in Figure **2**, where a bi-linear representation is suggested. The concept of crack closure can be used to explain this response, as for example in the models of Schmit and Paris **[17]** and Beevers **[18]**. Each threshold value is considered to be the sum of the intrinsic barrier to fatigue crack growth and the resistance to the crack growth arising from the presence of crack closure. Alternatively, the response may be explained in terms of the behaviour at the crack tip The initial fall is associated with a constant value of crack tip opening displacement **[19]**, whilst the limiting threshold value occurs when maximum tip root radius exceeds a critical value, so causing the crack to behave as a blunt notch **[20]**. The same data is presented in Figure **3** in the alternative form suggested by Marci **[21]** Marci et al **[22]** and Doker **[23]** who suggested that the threshold data fell with an envelope defined by a vertical and a horizontal line, which in this case have been drawn at ΔK_{th} = 2.2 MPa$\sqrt{m}$ and $K_{max,th}$ = 6 MPa$\sqrt{m}$, respectively.

The near-threshold fatigue crack growth rates associated with HCF cycles have been determined for stress ratios of 0.75, 0.82 and 0.90. Two procedures were used. First, measurement following the determination of the fatigue threshold value using HCF cycles only and a load shedding sequence, and second, derivation from the overall growth rates for HCF/LCF loadings by the method of back calculation. Generally, there is good

agreement between the results of these two procedures, showing that there is no significant load interaction effect (Figures **4-6**). The exception is the case of the retardation evident in the growth rates derived for HCF/LCF test involving a HCF stress ratio (R_{HCF}) of 0.90 with 1000 HCF cycles per LCF cycle. When this particular data set is removed, the remaining data for R_{HCF}= 0.90 are seen to be in good agreement (Figure **7**). The HCF crack growth rates for R_{HCF}= 0.75 and 0.82 and 0.90 have been represented by fits to the data in which $y = da/dB_{HCF}$ and $x = \Delta K_{HCF}$. These representations are visually fitted polynomial equations whose coefficients show a simple and small variation with R_{HCF}; the results being illustrated in Figure **8**, and the coefficients being recorded in Table **1**.

Table **1.** Coefficients of the polynomial fits to the HCF crack growth rate data

R_{HCF}	x^3	x^2	x^1	x^0
0.75	4×10^{-8}	-2×10^{-7}	6.00×10^{-7}	-1×10^{-6}
0.82	4×10^{-8}	-2×10^{-7}	6.58×10^{-7}	-1×10^{-6}
0.90	4×10^{-8}	-2×10^{-7}	6.95×10^{-7}	-1×10^{-6}

2.2 LCF crack growth rates

The fatigue crack growth rates associated with the application of separate LCF cycles have been determined for values of ΔK_{LCF} in the range 12-50 MPa$\sqrt{}$m (Figure **9**). The results exhibit a clearly defined bilinear response, with the transition occurring at ΔK_{LCF} = 20 MPa$\sqrt{}$m. In keeping with the concepts proposed by Yoder et al [**24-26**] and Yeun et al [**27**], a good correlation is found between the calculated reversed plastic zone size and the primary alpha grain size of the alloy, these being 21μm and 23 μm respectively. The mean of the data can be represented by the relationships:

$$da/dN_{LCF} = 1.770 \times 10^{-11} [\Delta K_{LCF}]^{5.468} \quad \text{for } \Delta K_{LCF} = 12 - 20 \quad ...(1)$$

$$da/dN_{LCF} = 1.284 \times 10^{-8} [\Delta K_{LCF}]^{3.269} \quad \text{for } \Delta K_{LCF} = 20 - 40 \quad ...(2)$$

where da/dN_{LCF} is measured in mm / cycle and ΔK_{LCF} in MPa$\sqrt{m}$

A scatter band has been drawn that encompasses 95% of the data. This scatter band has a width of 2.7, that is to say, the ratio of the fatigue crack growth rate at the upper bound to that at the lower bound, for a fixed value of ΔK, is 2.7

2.3 HCF/LCF crack growth rates

The fatigue crack growth rate data for combinations of HCF and LCF cycles are presented in Figure **10-12**, the growth rate per applied loading block, $da/dB_{HCF/LCF}$, being plotted as a function of the peak-to-peak stress intensity range, ΔK_{LCF}, for the combined loading. Each figure shows the data for a fixed value of R_{HCF} in comparison with the data for LCF cycles only. Up to three values of N_{HCF}, the number of HCF cycles in each loading block, are considered, N_{LCF} being set at 1. The majority of the results are for CT specimens and the remainder for CN specimens. The effect of the different variables are as follows. First, with regard to R_{HCF}, the lower its value the lower is the value of ΔK_{LCF} at which regime 2 growth is observed, and the greater the subsequent enhancement in growth rate relative to that for LCF cycles only. Second, with regard to the value of n, the greater its value the greater the crack growth rate in regime 2. Third, with regard to specimen design, there is no significant effect.

3. Predictions of crack growth response under combined LCF/HCF loadings

The methodology used to predict the fatigue crack growth rate for the combined HCF/LCF loadings of interest depends upon whether or not the HCF cycles are preceded by an overload cycle. In the absence of an overload, the da/dB values are estimated by the linear summation rule:

$$da/dB = da/dB_{HCF} + da/dB_{LCF} \quad ...(3)$$

or:

$$da/dB = N_{HCF} \times da/dN_{HCF} + N_{LCF} \times da/dN_{LCF} \quad ...(4)$$

The values of da/dN_{HCF} used in these predictions are those represented by the polynomial for $R_{HCF} = 0.82$ given in Table 1, whilst the values of da/dN_{LCF} are those represented by the mean of the data for $R_{LCF} = 0.1$ given in equations 1 and 2. When the HCF cycles are preceded by a overload LCF cycle, the Wheeler model is used to modify the contribution to the crack growth from the HCF cycles. All the results are plotted as log (da/dB) versus log (ΔK_{HCF}), with the results for the LCF component of the loading (da/dB_{LCF}) included for comparison.

Figure **13** gives a schematic representation of the repeated stress - time sequences which have been considered, the various loading blocks being classified according to the number and form of the LCF cycles. Thus:

Type A has a single LCF cycle which underloads the following HCF cycles,

Type B has multiple LCF cycles which underload the following HCF cycles,

Type C has a single LCF cycle which overloads the following HCF cycles,

Type D has multiple LCF cycles which overload the following HCF cycles,

Different numbers of HCF cycles within the loading block are also considered.

3.1 Effect of N_{HCF} per block

Figure **14** shows the predicted response to a sequence of HCF/LCF loadings involving a single LCF underload cycle in combination with 100, 1000 and 10 000 HCF cycles per loading block. These predictions confirm the experimental results for such conditions [**14**] namely, a constant value of ΔK_{onset}, and within regime 2, a progressively increasing da/dB with increasing N_{HCF}.

3.2 Effect of N_{LCF} per block

Figures **15** and **16** relate to a sequence of HCF/LCF loadings involving a multiple LCF underload cycle in combination with 1000 and 10 000 HCF cycles per loading block,

respectively. Increasing the number of LCF underload cycles has two effects. First, a progressive increase in da/dB_{LCF} in decade steps as N_{LCF} is increased in decade steps. Second, the difference between da/dB_{LCF} and da/dB decreases as the proportion N_{LCF} to N_{HCF} increases.

3.3 Effect of overload LCF cycles

The effect of crack growth retardation due to the presence of a single LCF overload cycle used in conjunction with 1000 and 10 000 HCF cycles per loading block is shown in Figures **17** and **18** respectively. Each figure show that progressively increasing the Wheeler constant leads to the reduction and eventual suppression of the HCF contribution to crack growth. Figure **19** illustrates the result of multiple LCF overloads. In this case the number of HCF cycles per block is set at 1000 and the Wheeler constant set at 6. Once more there is both a progressive increase in da/dB_{LCF} in decade steps as N_{LCF} is increased in decade steps; and the difference between da/dB_{LCF} and da/dB decrease as the proportion N_{LCF} to N_{HCF} increases.

4. Development of the test facility

The test facility was designed to apply the repeated loading indicated as type A in Figure 13, and it has been modified in order that the loadings indicated as types B, C and D, can be applied. These modifications also enable the determination of fatigue thresholds for HCF crack growth for conditions involving either gradual or substantial load shedding sequences. The two features which required alteration were the air bag isolation unit and the control system for the machine, the latter leading to a new system for monitoring the crack growth test data. In addition, the recent UK Health and Safety regulations required the existing cooling system to be replaced by one which is totally enclosed.

4.1 Modifications to the isolation unit

The function of the air bag unit is to decouple the electromagnetic actuator, which applies the HCF cycles, from the servohydraulic actuator, which provides the LCF loading. This allows the two actuators to function simultaneously and without interaction. The new design

incorporates a parallel load path into the isolation unit. When the HCF cycles are applied this parallel load path is not engaged, and the isolation unit functions in the normal manner. The parallel load path comes into operation only during the application of a LCF cycle which involves an overload. In this way the required high loading is applied to the specimen without excessive compression of the air bag.

4.3 New control and monitoring system

The new system of load control and data collection is computer based. The development of the system was achieved by interfacing the computer with the existing analogue control console [via a D to A interface card], interfacing with a multi-channel digital voltmeter [via a GPIB card], and interfacing with the DC power supply [via a relay card]. The performance of the computer was upgraded and a data protection facility in the form of an uninteruptable power supply [American Power Conversion] was provided. Testpoint software [Capital Equipment Corp] was installed and programs written which would control and monitor the tests for the various load - time sequences specified in the study.

In the previous system the load levels and ramp rates were set by analogue controls, whilst the LCF and HCF waveforms were fixed. A data logger was used to control the pulsing of the DCPD crack monitoring system, to monitor the test systems and to record the test data as hard copy only. With the new system the load levels, ramp rates and LCF waveform are all determined by the computer software, which permits manual fine tuning of the selected load levels. In addition, the computer controls the pulsing of the DCPD crack monitoring system, the monitoring of the test systems, and the recording of the test data as Excel and text files.

5. Conclusions

1. The results of past studies on the effect of HCF and LCF loadings, both when applied separately and in combination, on the fatigue crack growth rate behaviour of forged Ti-6Al-4V have been re-analysed. Equations representing the HCF and LCF crack growth rates

were determined, together with the limiting values of the maximum stress intensity and the range of stress intensity associated with the threshold condition for HCF crack growth.

2. Fatigue crack growth rates for combined LCF/HCF loading experiments involving systematic variations in the ratio of HCF to LCF cycles within each repeated loading block have been predicted. The predictions indicate the manner in which the contribution to the overall growth rate from the HCF cycles declines as the ratio of HCF cycles to LCF cycles is reduced, and overloading of the HCF cycles by the LCF cycles retards the HCF crack growth.

3. A test facility able to apply a wide range of HCF/LCF loadings has been achieved through the modification of the HCF/LCF isolation unit and the installation of new load control and test monitoring systems.

References

1. **Powell, B. E., Hall, R. F. and Hawkyard, M.** "The effect of superimposed vibrational stresses on fatigue crack propagation life", In: *1st Int. Conf. on Structural Integrity Assessment,* Manchester, 1992, 336-345.

2. **Powell, B. E.** "Crack growth in Ti-6Al-4V under the conjoint action of high and low cycle fatigue", *Int. J. Fatigue,* 1987, **9**, 195-202.

3. **Powell, B. E.** "Fatigue crack growth behaviour of two contrasting titanium alloys", *Int. J. Fatigue,* 1995, **17**, 221-227.

4. **Specht, J. U.** "The low cycle fatigue behaviour of titanium alloys", In: *3rd Int. Conf. on Low Cycle Fatigue and Elastoplastic Behaviour of Materials,* Berlin, 1992, 19-24.

5. **Powell, B. E., Henderson, I. and Duggan, T. V.** "The effect of combined major and minor stress cycles on fatigue crack growth", In: *2nd Int. Conf. on Fatigue and Fatigue Thresholds,* Birmingham, EMAS, Warley, UK, 1984, **2**, 893-902.

6. **Hawkyard, M., Powell, B. E., Hussey, I. and Grabowski, L.** "Fatigue crack growth under the conjoint action of major and minor stress cycles", *Fatigue Fract. Eng. Mater. Strut.,* 1996, **19**, 217-227.

7. **Claridge, S. P. and Powell, B. E.** "Fatigue crack growth life predictions for single and dual amplitude loadings", In: *1st Int. Conf. on Computational Methods and Testing for Engineering Integrity*, Computational Mechanics Publications, Southampton, UK, 1996, 87-96.

8. **Evans, W. J., Medwell, N. and Spence, S. H.** "The effect of major-minor cyclic combinations on crack propagation lifing criteria", In: *12th Int. Symp. on Air Breathing Engines American Institute of Aeronautics and Astronautics,* 1995, **1**, 185.

9. **Powell, B. E. and Duggan, T. V.** "Predicting the onset of high cycle fatigue damage: an application for long crack threshold data", *Int. J. Fatigue,* **8**, 1986, 187-194.

10 **Taghani, N. and Powell, B.E.** "Threshold testing for the vibration assessment of a turbine disc alloy", In: *4th Int. Conf. on Fatigue and Fatigue Thresholds*, Honolulu, Hawaii, 1990, **3**, 1387-1392.

11. **Hall, R. F. and Powell, B.E.** "The effect of temperature on the growth of cracks subjected to combined major and minor stress cycles", In: *Mechanical Behaviour of Materials, (Ed C Moura Branco, R Ritchie, and V Sklenicka)* Kluwer Academic Publishers, Dordrecht, The Netherlands, 1996, 227-235.

12. **Hawkyard, M. and Powell, B. E.** "Elevated temperature crack growth in a low alloy steel due to major and minor stress cycles", In: *11th European Conf on Fracture,* Poitiers, France, 1966. **2**, 1281-1286.

13. **Powell, B. E., Duggan, T. V. and Jeal, R. H.**, "The influence of minor cycles on low cycle fatigue crack propagation", *Int. J. Fatigue*, 1982, **4**, 4-14.

14. **Powell, B. E. and Duggan, T. V.,** " Crack growth in Ti-6Al-4V under the conjoint action of high and low cycle fatigue", *Int. J. Fatigue*, 1986, **9**, 195-202.

15. **Hall, R. F. and Powell, B. E.,** "The growth of corner cracks", *Int. J. Fatigue*, 1997, **19**, 429-435.

16 **Powell, B. E., Hawkyard, M. and Grabowski L.,** "The growth of cracks in Ti-6Al-4V plate under combined high and low cycle fatigue", *Int. J. Fatigue*, 1997, **19**, S167-S176.

17. **Schmit, R. A. and Paris, P.C.,** " Threshold for fatigue crack propagation and the effect of load ratio and frequency", In: *Progress in Flaw Growth and Fracture Toughness Testing*, ASTM STP 563, 1972, 79-94.

18. **Beevers, C. J.,** "Some aspects of the influence of microstructure and environment on ΔK threshold", In: *Fatigue Thresholds,* EMAS, Warley, U.K. 1981, **1**, 257-275.

19. **McEvily, A. J. and Groeger, J.,** "On the threshold for fatigue crack growth", In: *Proc. Conf. Fracture,* 1977, **2,** 1293-1298.

20 **Braid, J.E.M., Taylor, D. and Knott, J.F.,** "A model for fatigue thresholds at high R ratios". *Canadian Metall. Quart.,* 1987, **26**, 161-165.

21. **Marci, G.,** "Non-propagation conditions (ΔK_{th}) and fatigue crack propagation thresholds (ΔK_T)", *Fatigue Fract. Engng. Mater. Struct.,* 1994, **17**, 891-907.

22. **Marci, G., Castro, D.E. and Bachmann V.,** "Fatigue crack propagation threshold", *Journal of Testing and Evaluation,* 1989, **17**, 28-39.

23 **Doker H.,** "Fatigue crack growth threshold: implications, determination and data evaluation", *Int. J. Fatigue*, 1997, **19**, S145-S149.

24 **Yoder, G.R., Cooley, L.A. and Crooker, T. W.,** *Titanium 80:Science and Technology,* Metallurgical Society AIME, New York, 1980, 1865.

25 **Yoder, G.R., Cooley, L.A. and Crooker, T. W.,** *Engineering Fracture Mechanics,* 1979, **11**, 805.

26 **Yoder, G.R., Cooley, L.A. and Crooker, T. W.,** *Metallurgical Transactions,* 1977, **8A**, 1737.

27 **Yuen, A., Hopkins, S. W., Leverant, G. R. and Rau, C. A.,** *Metallurgical Transactions,* 1974, **5**, 1833.

Figures

Figure 1. Form of fatigue crack growth rate curve for a simple HCF/LCF loading combination

Figure 2. Effect of stress ratio on the room temperature fatigue threshold value of forged Ti-6Al-4V

Figure 3. K_{max} dependence of the room temperature fatigue threshold value of forged Ti-6Al-4V

Figure 4 Comparison of back calculated HCF crack growth rates for $R_{HCF} = 0.75$ from HCF/LCF tests at n = 1000:1 and n = 10 000:1, with crack growth data measured following the determination of the threshold value by a load shedding procedure

Figure 5 Comparison of back calculated HCF crack growth rates for $R_{HCF} = 0.82$ from HCF/LCF tests at n = 1000:1 and n = 10 000:1, with crack growth data measured following the determination of the threshold value by a load shedding procedure

Figure 6 Comparison of back calculated HCF crack growth rates for $R_{HCF} = 0.90$ from HCF/LCF tests at n = 1000:1, n = 10 000:1 and n = 100 000:1, with crack growth data measured following the determination of the threshold value by a load shedding procedure

Figure 7 Comparison of back calculated HCF crack growth rates for $R_{HCF} = 0.90$ from HCF/LCF tests with n = 10 000:1 and n = 100 000:1, with crack growth data measured following the determination of the threshold value by a load shedding procedure

Figure 8 Comparison of near-threshold crack growth rates representations for R_{HCF} = 0.75, 0.82 and 0.90

Figure 9 Fatigue crack growth rates for LCF cycles at R_{LCF} = 0.1 with representation of the test data by scatterband

Figure 10 Comparison of HCF/LCF crack propagation data for R_{HCF} = 0.75 at n = 1000:1 and 10 000:1, with the scatterband representing the LCF cycles only

Figure 11 Comparison of HCF/LCF crack propagation data for R_{HCF} = 0.82 at n = 1000:1 and 10 000:1, with the scatterband representing the LCF cycles only

Figure 12 Comparison of HCF/LCF crack propagation data for R_{HCF} = 0.90 at n = 1000:1, 10 000:1 and 100 000:1, with the scatterband representing the LCF cycles only

Figure13 Schematic representation of the repeated stress - time sequences considered

Figure 14(a) The effect of the number of HCF cycles - crack growth with a loading block of n = 100:1

Figure 14(b) The effect of the number of HCF cycles - crack growth with a loading block of n = 1000:1

Figure 14(c) The effect of the number of HCF cycles - crack growth with a loading block of n = 10 000:1

Figure 15(a) The effect of the number of LCF cycles - crack growth with a loading block of n = 1000:1

Figure 15(b) The effect of the number of LCF cycles - crack growth with a loading block of n = 1000:10

Figure 15(c) The effect of the number of LCF cycles - crack growth with a loading block of n = 1000:100

Figure 16(a) The effect of the number of LCF cycles - crack growth with a loading block of n = 10 000:1

Figure 16(b) The effect of the number of LCF cycles - crack growth with a loading block of n = 10 000:10

Figure 16(c) The effect of the number of LCF cycles - crack growth with a loading block of n = 10 000:100

Figure 16(d) The effect of the number of LCF cycles - crack growth with a loading block of n = 10 000:1000

Figure 17(a) The effect of Wheeler's constant - crack growth with w = 1 and a loading block of n = 1000:1

Figure 17(b) The effect of Wheeler's constant - crack growth with w = 6 and a loading block of n = 1000:1

Figure 17(c) The effect of Wheeler's constant - crack growth with w = 12 and a loading block of n = 1000:1

Figure 18(a) The effect of Wheeler's constant - crack growth with w = 1 and a loading block of n = 10 000:1

Figure 18(b) The effect of Wheeler's constant - crack growth with w = 6 and a loading block of n = 10 000:1

Figure 18(c) The effect of Wheeler's constant - crack growth with w = 12 and a loading block of n = 10 000:1

Figure 19(a) The effect of the number of LCF overload cycles - crack growth with w = 6 and a loading block of n = 1000:1

Figure 19(b) The effect of the number of LCF overload cycles - crack growth with w = 6 and a loading block of n = 1000:10

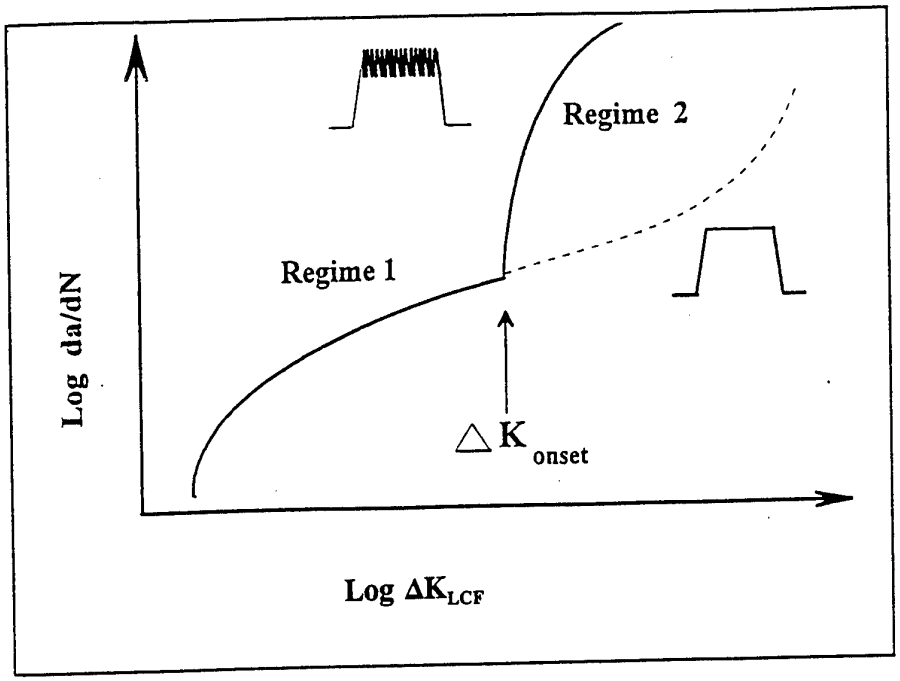

Figure 1. Form of fatigue crack growth rate curve for a simple HCF/LCF loading combination

Figure 2 Effect of stress ratio on the room temperature fatigue threshold value of forged Ti-6Al-4V

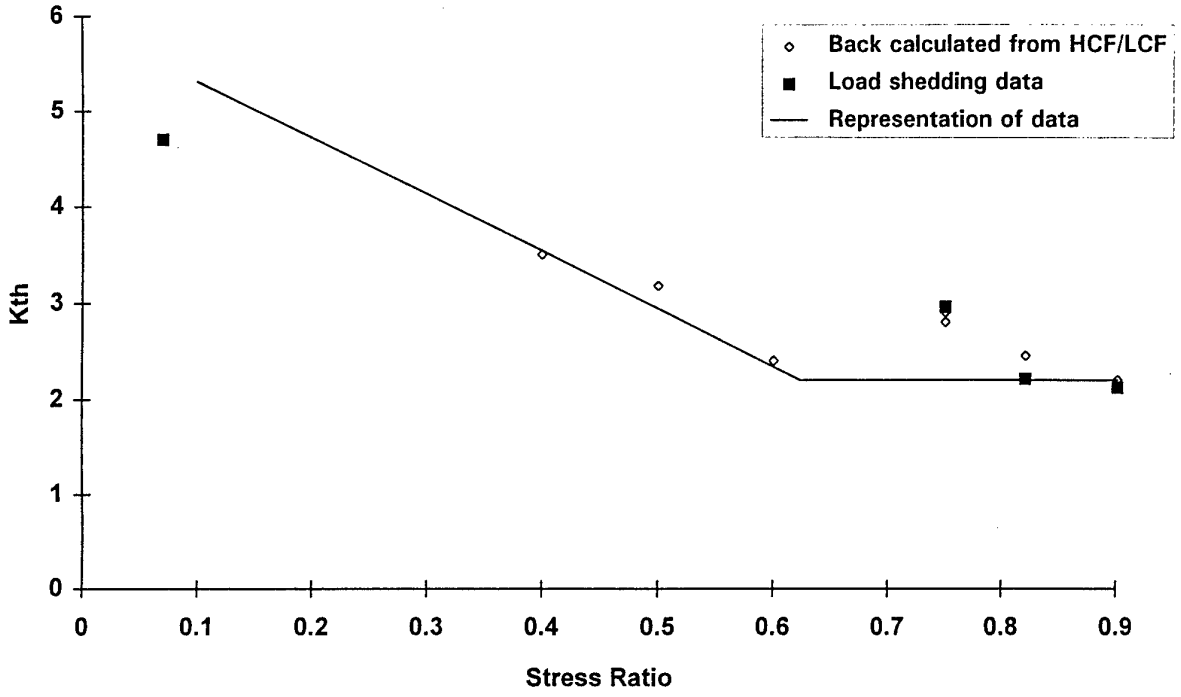

Figure 3 K_{max} dependence of the room temperature fatigue threshold value of forged Ti-6Al-4V

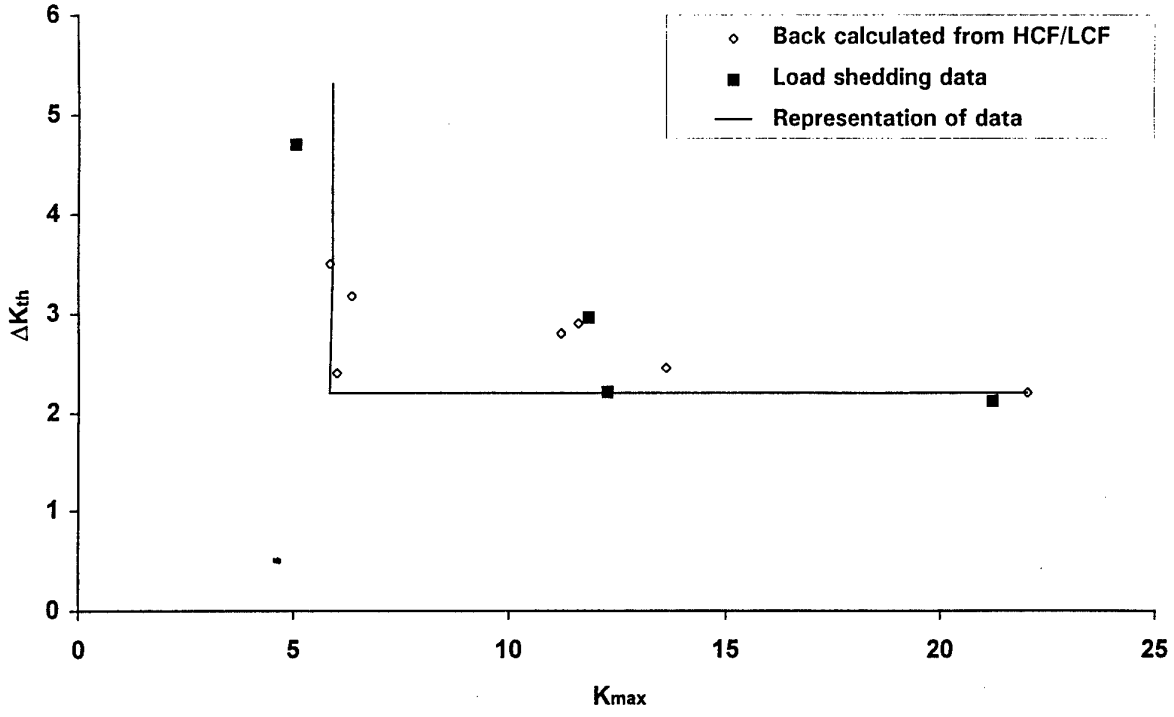

Figure 4 Comparison of back calculated HCF crack growth rates for R_{HCF}=0.75 from HCF/LCF tests with n=1000:1 and n=10 000:1, with crack growth data measured following the determination of the threshold value by a load shedding procedure.

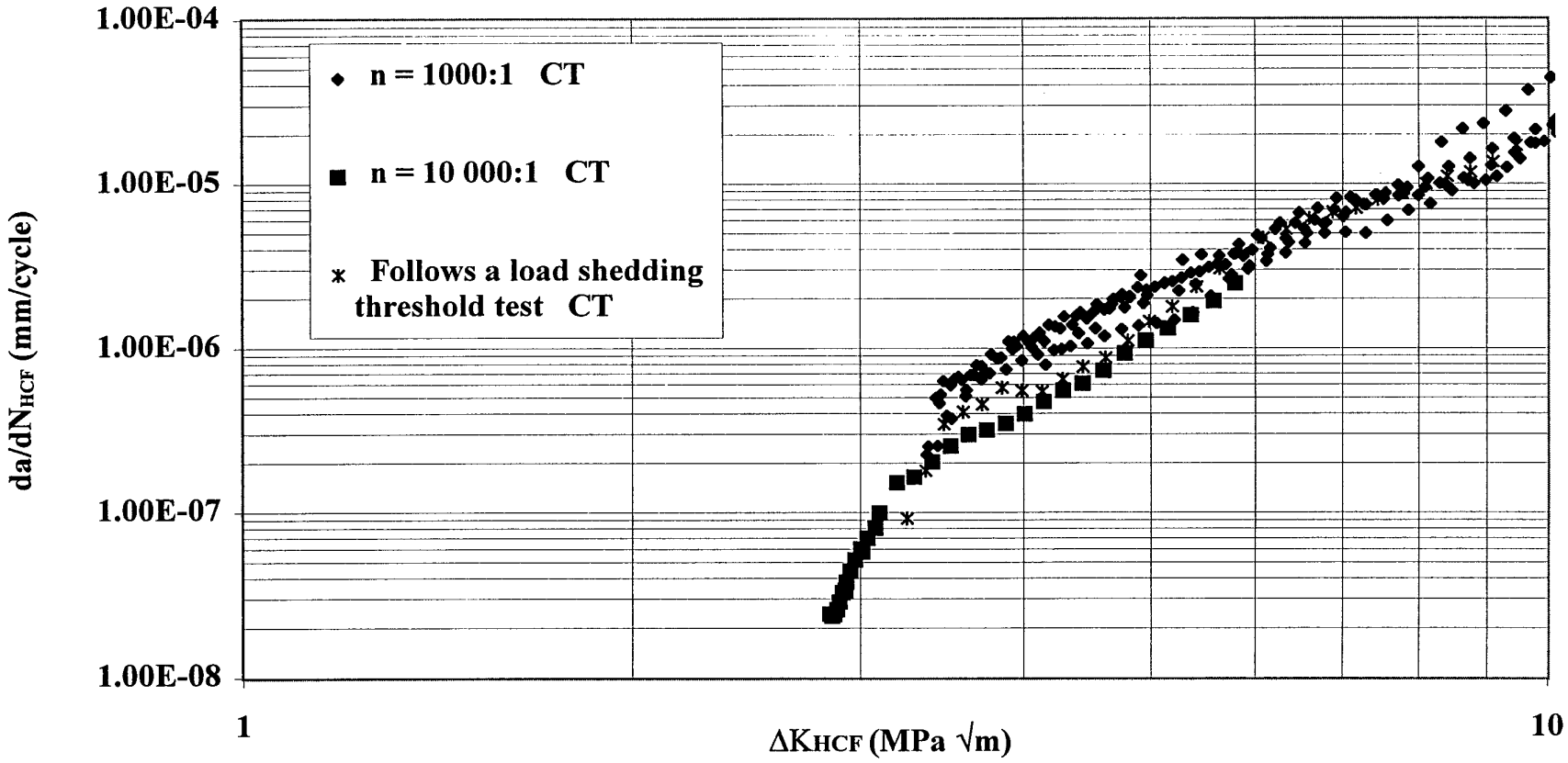

Figure 5 Comparison of back calculated HCF crack growth rates for R_{HCF}=0.82 from HCF/LCF tests at n=1000:1 and n=10 000:1, with crack growth data measured following the determination of the threshold value by a load shedding procedure

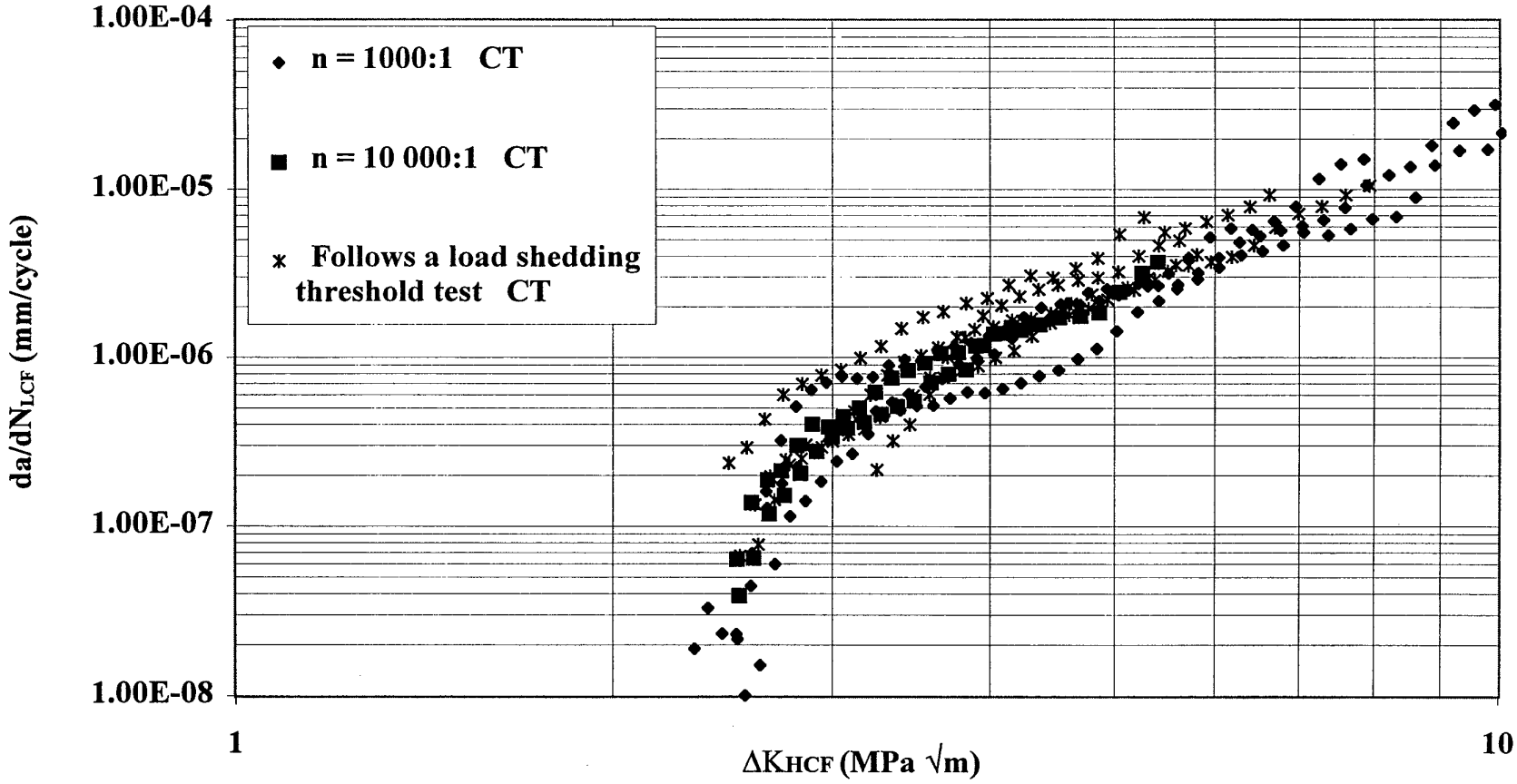

Figure 6 Comparison of back calculated HCF crack growth rates for R_{HCF}=0.90 from HCF/LCF tests at n=1000:1, n=10 000:1 and n=100 000:1, with crack growth data measured following the determination of the threshold value by a load shedding procedure.

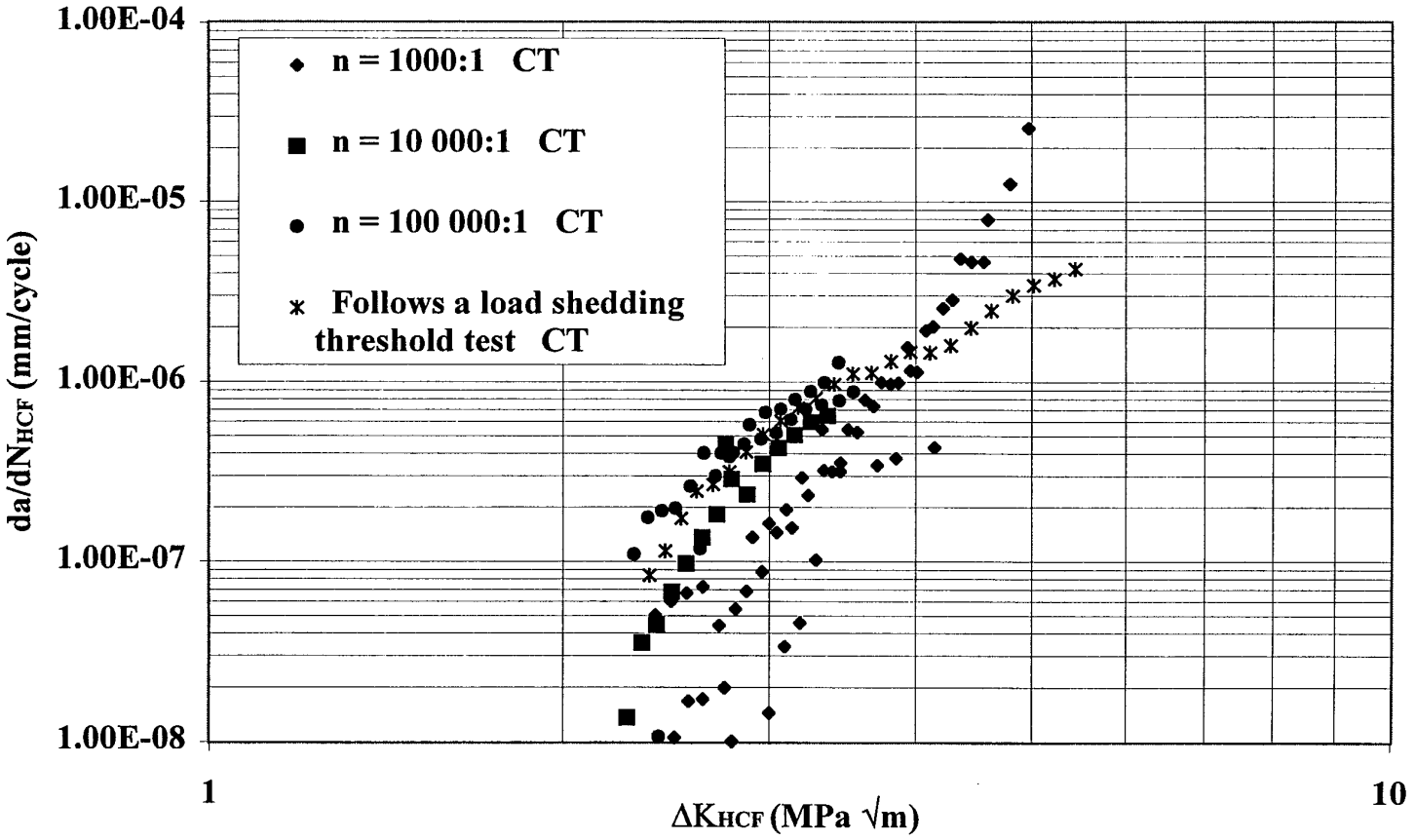

Figure 7 Comparison of back calculated HCF crack growth rates for R_{HCF}=0.9 from HCF/LCF tests at n=10 000:1 and n=100 000:1, with crack growth data measured following the determination of the threshold value by a load shedding procedure

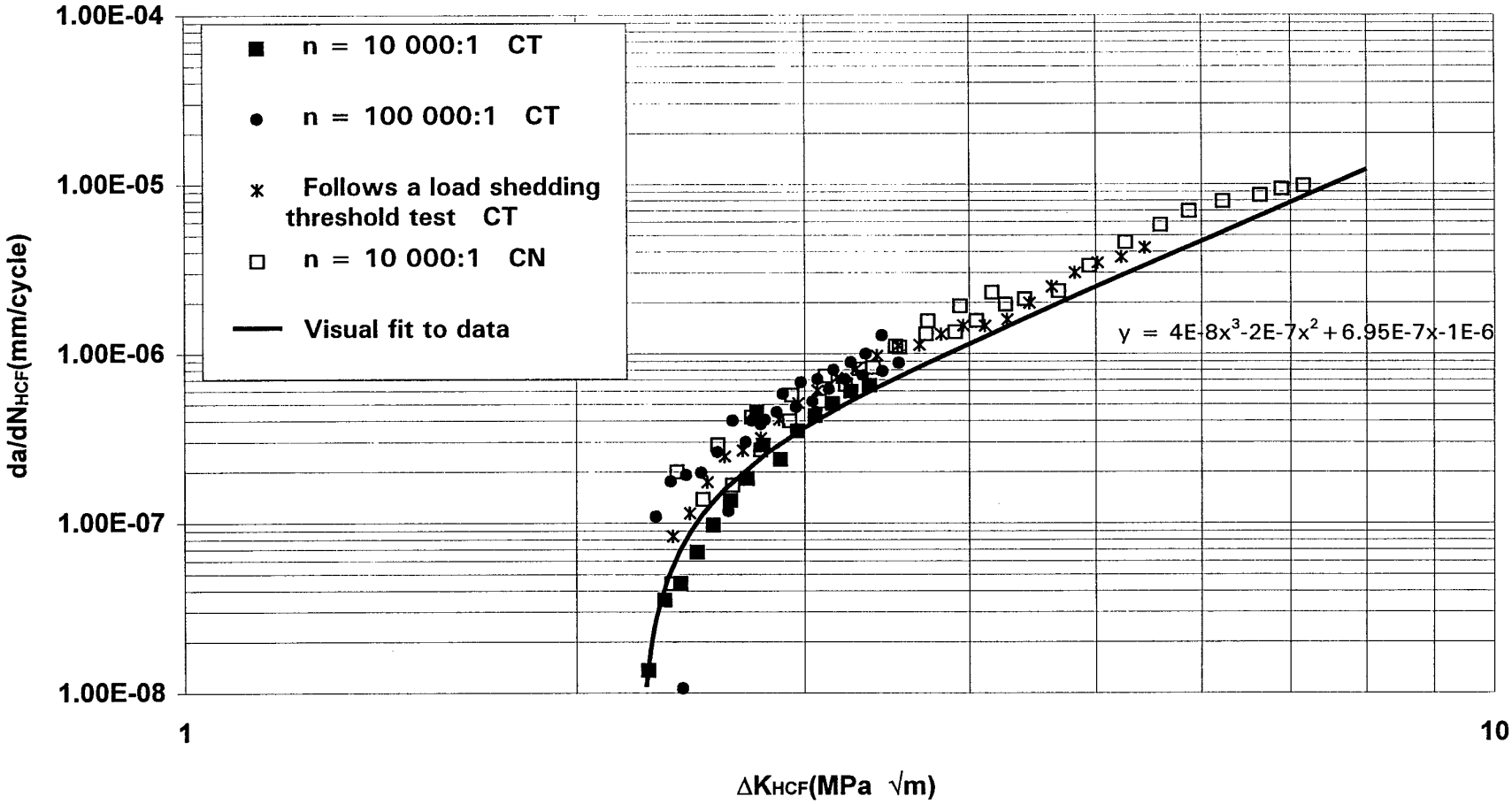

Figure 8 Comparison of near-threshold crack growth rate representations

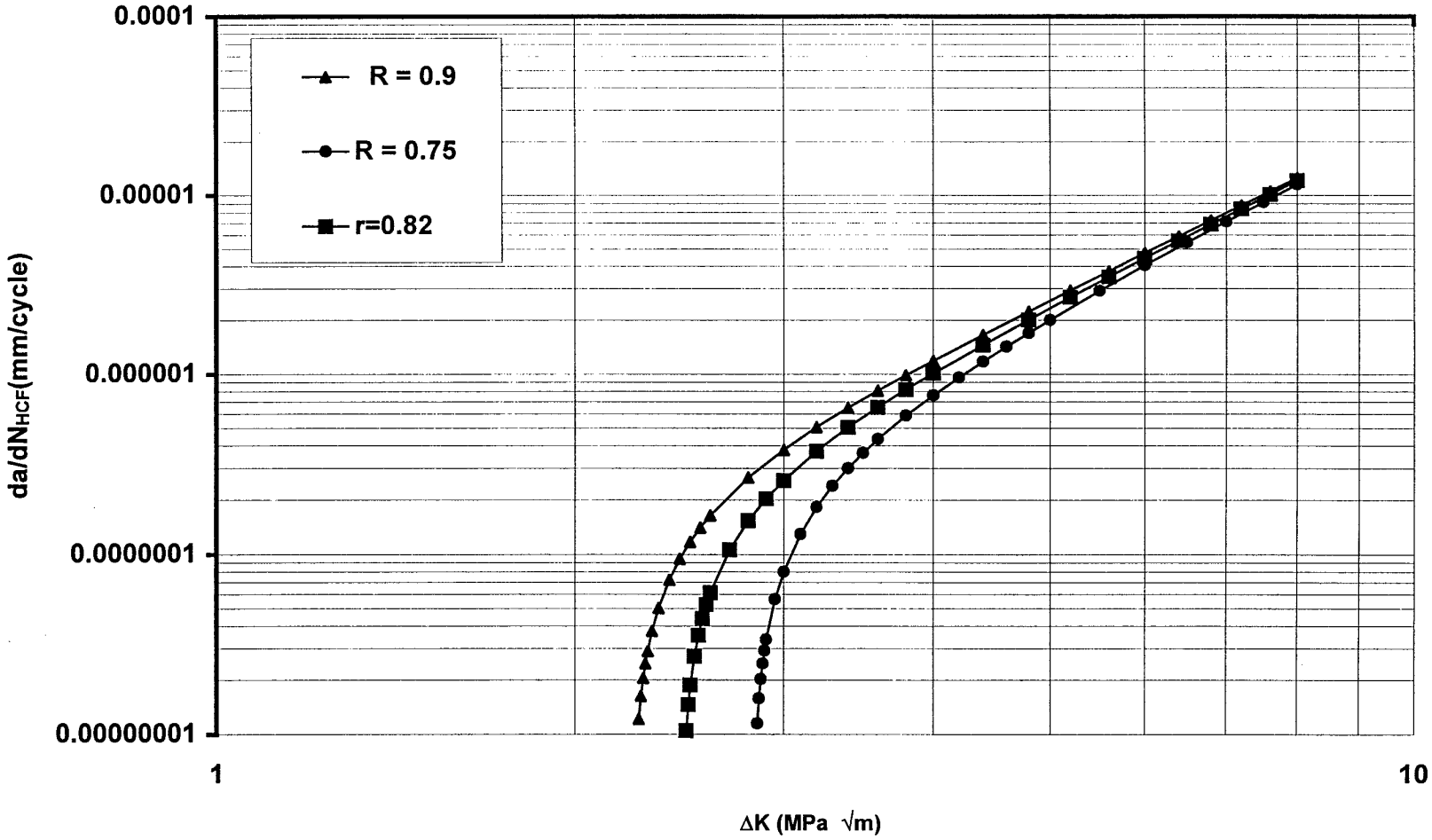

Figure 8 Comparison of near-threshold crack growth rate representations

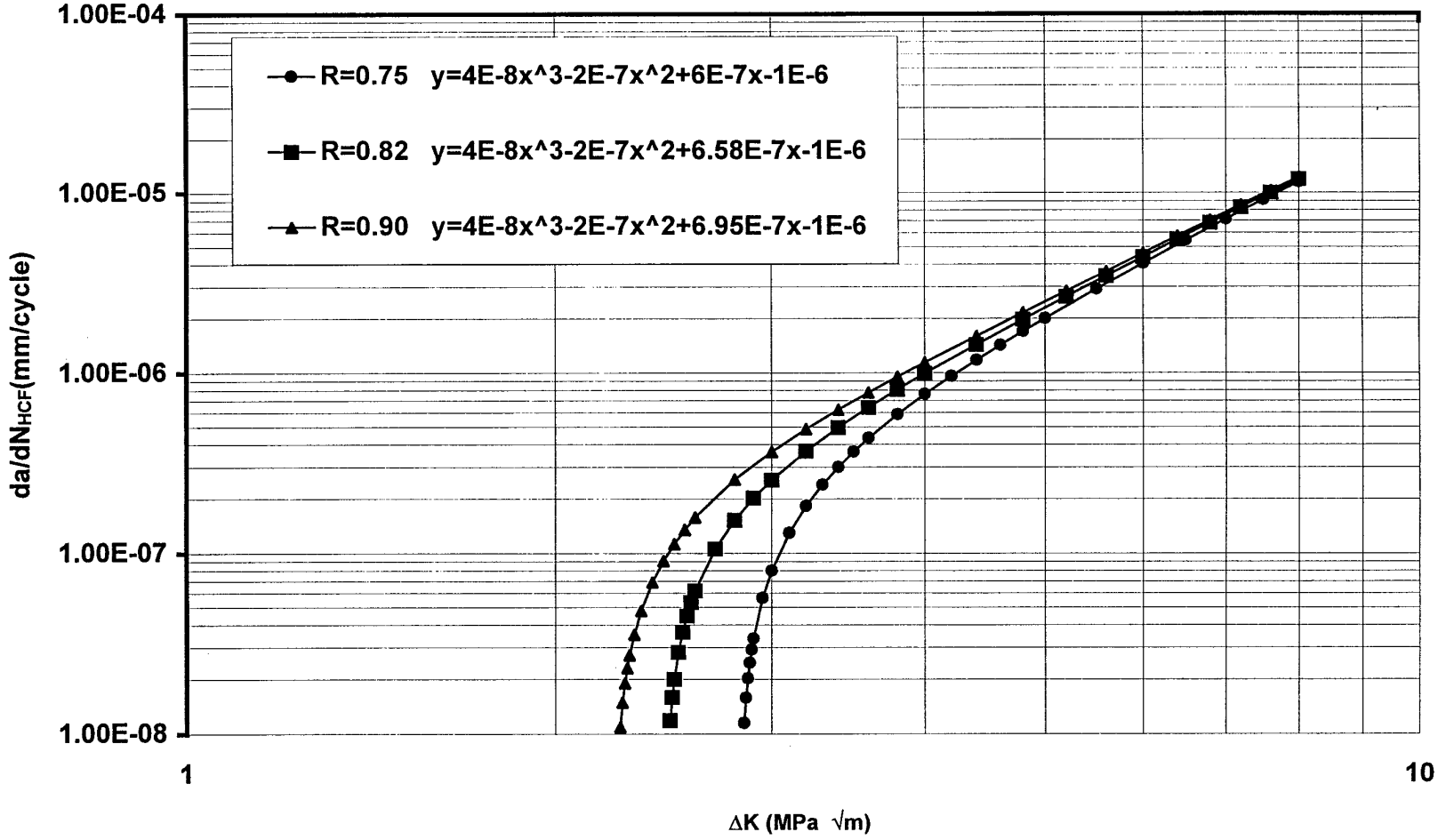

Figure 9 Fatigue crack growth rates for LCF cycles at R_{LCF}=0.1, with representation of test data by a scatter band.

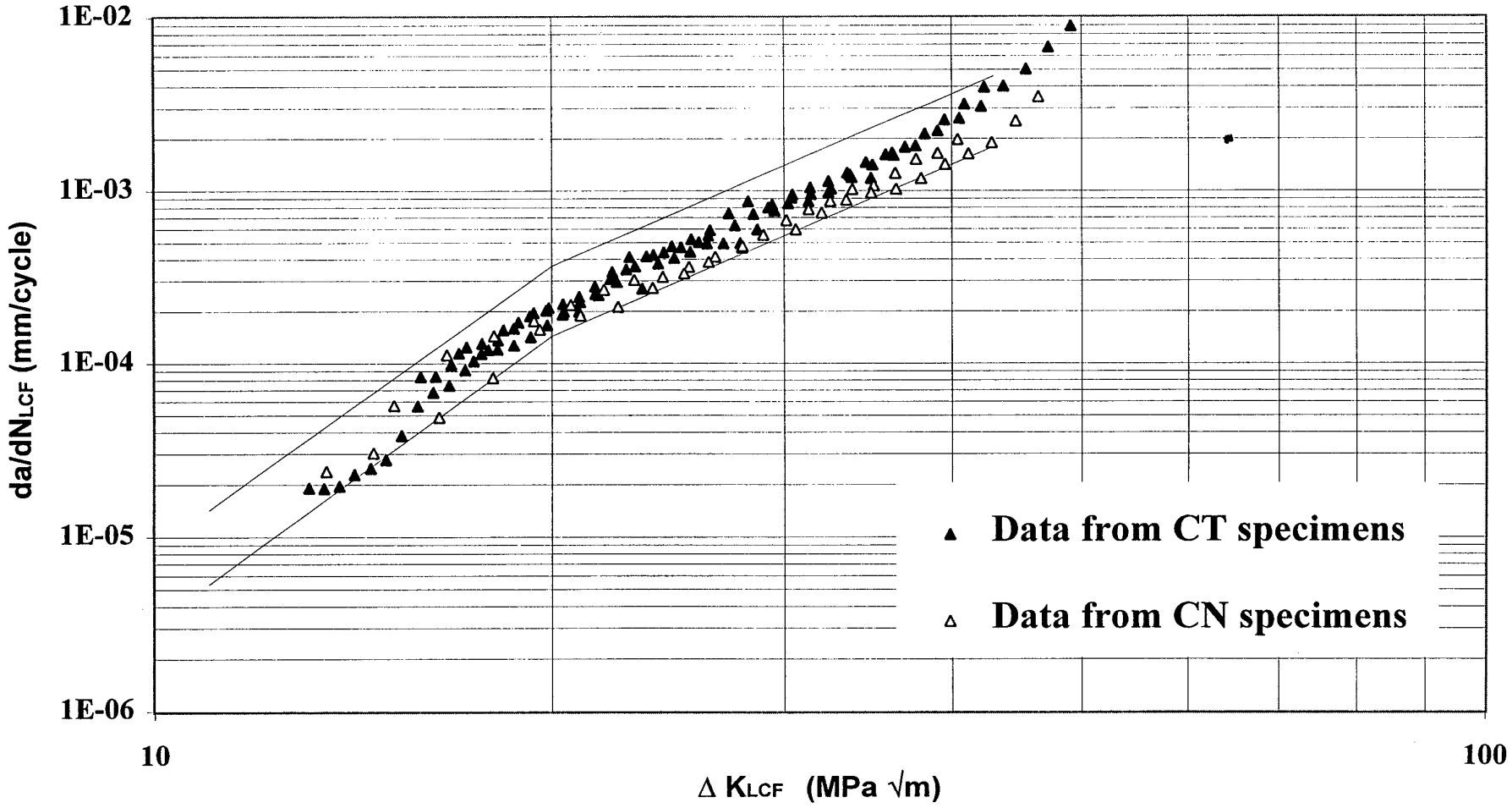

Figure 10 Comparison of HCF/LCF crack propagation data for R_{HCF}=0.75 at n= 1000:1 and n=10 000:1, with the scatterband representing the LCF cycles only.

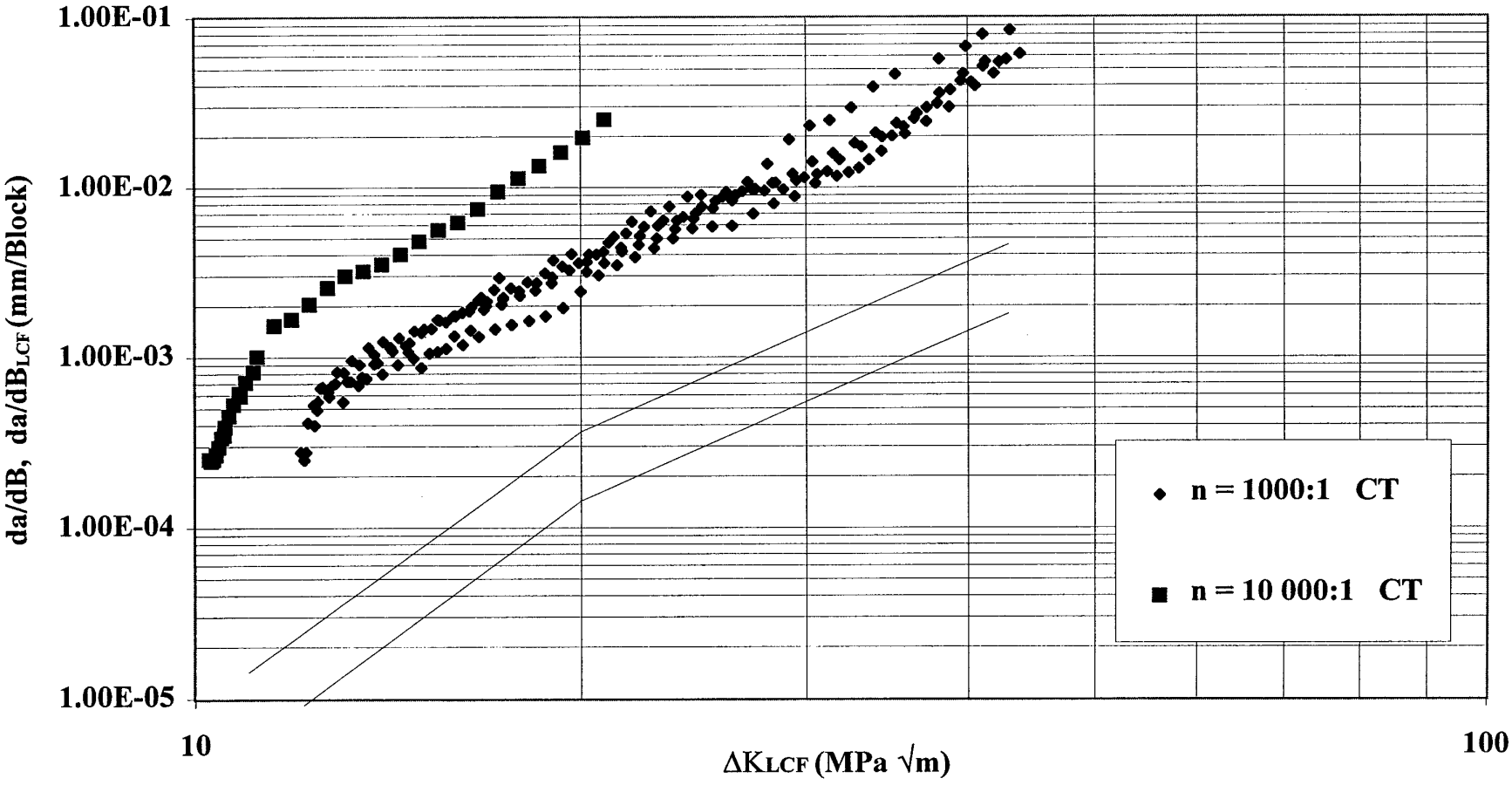

Figure 11 Comparison of HCF/LCF crack propagation data for R_{HCF}=0.82 at n=1000:1 and n=10 000:1, with the scatterband representing the LCF cycles only

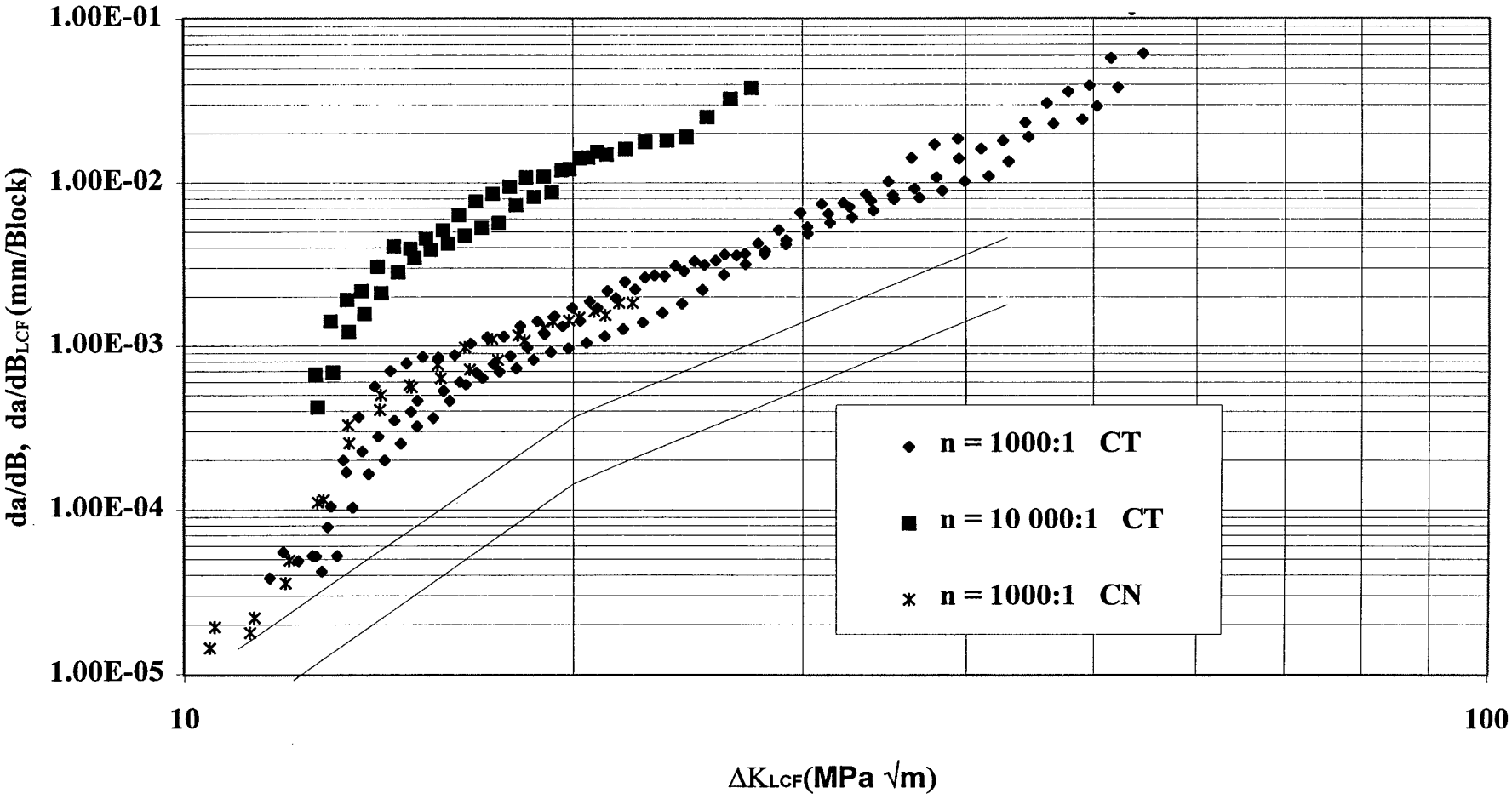

Figure 12 Comparison of HCF/LCF crack propagation data for R_{HCF}=0.9 at n=1000:1, n=10 000:1 and n=100 000:1, with the scatterband representing the LCF cycles only

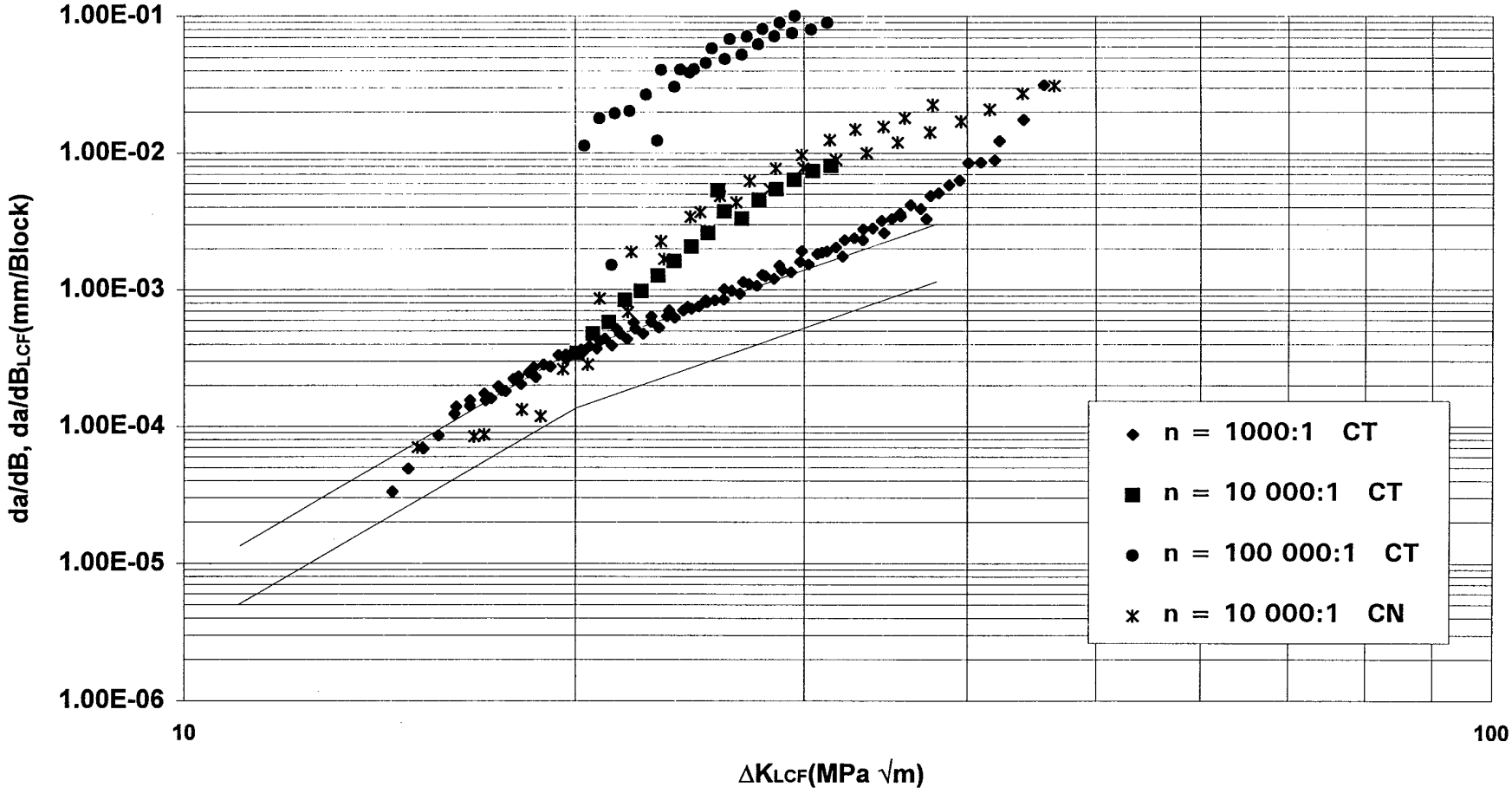

Figure 13 Schematic representation of the repeated stress - time sequences considered

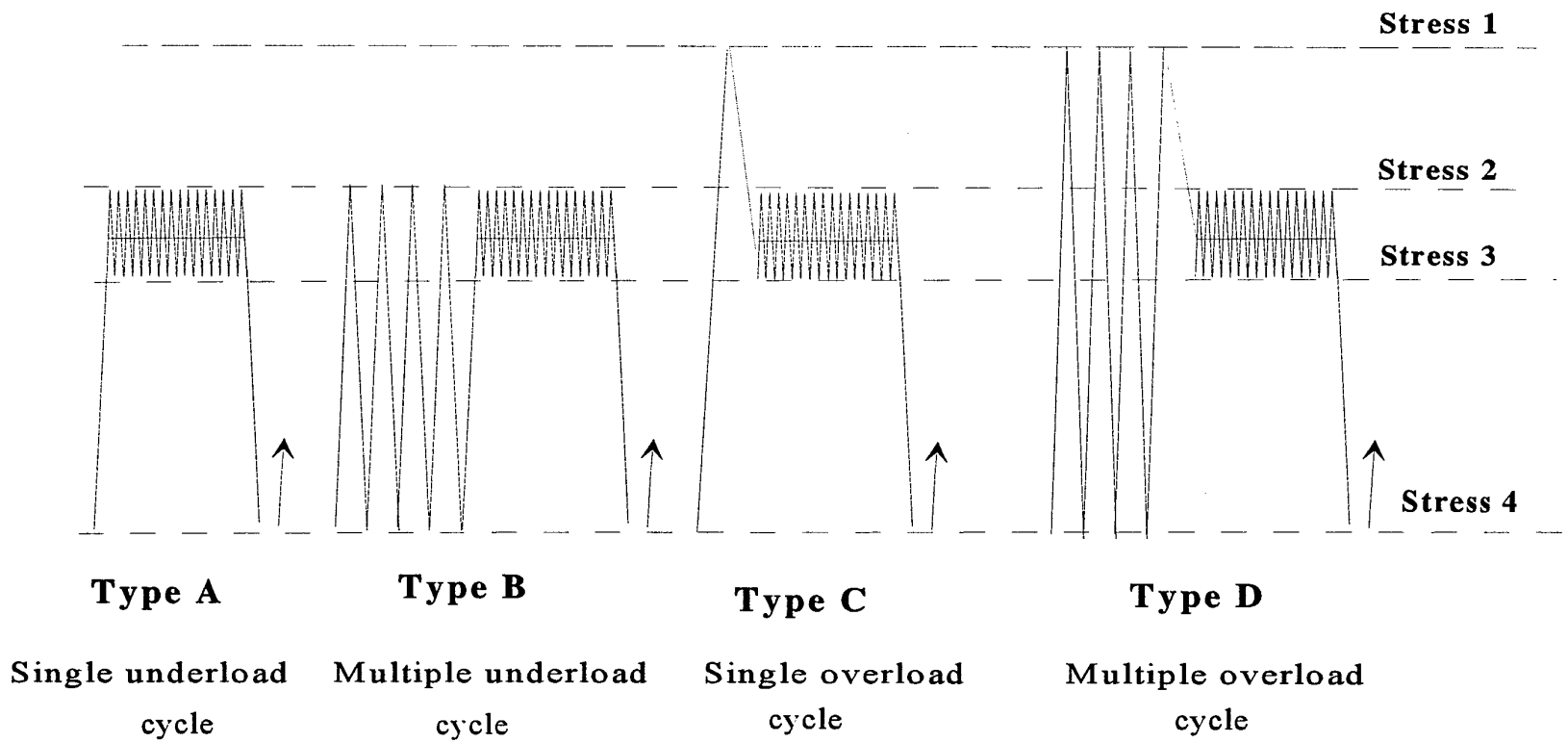

Figure 14(a) The effect of the number of HCF cycles - crack growth with a loading block of n = 100:1

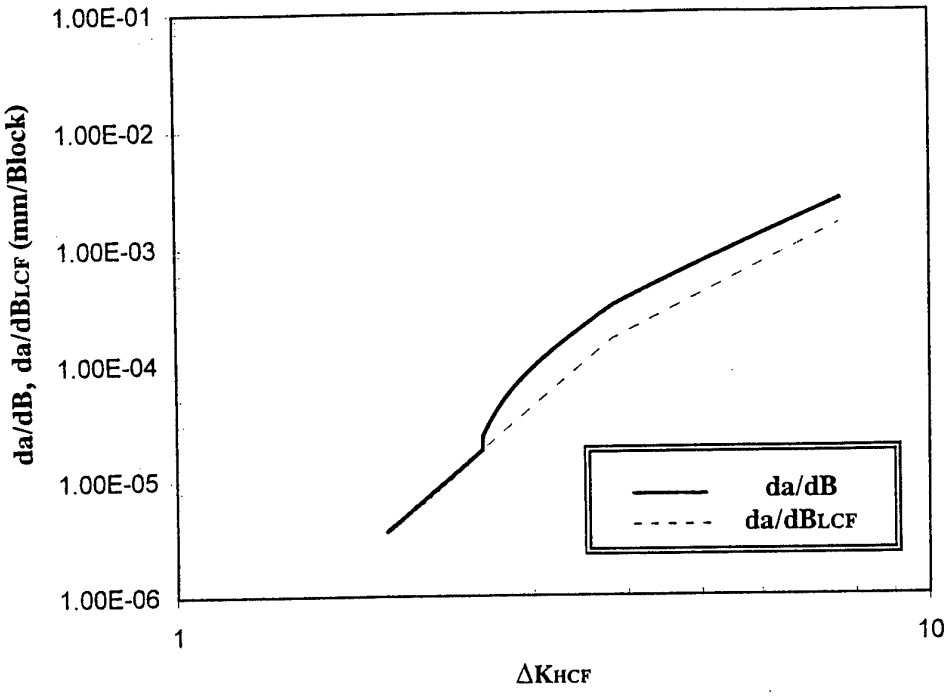

Figure 14(b) The effect of the number of HCF cycles - crack growth with a loading block of n = 1000:1

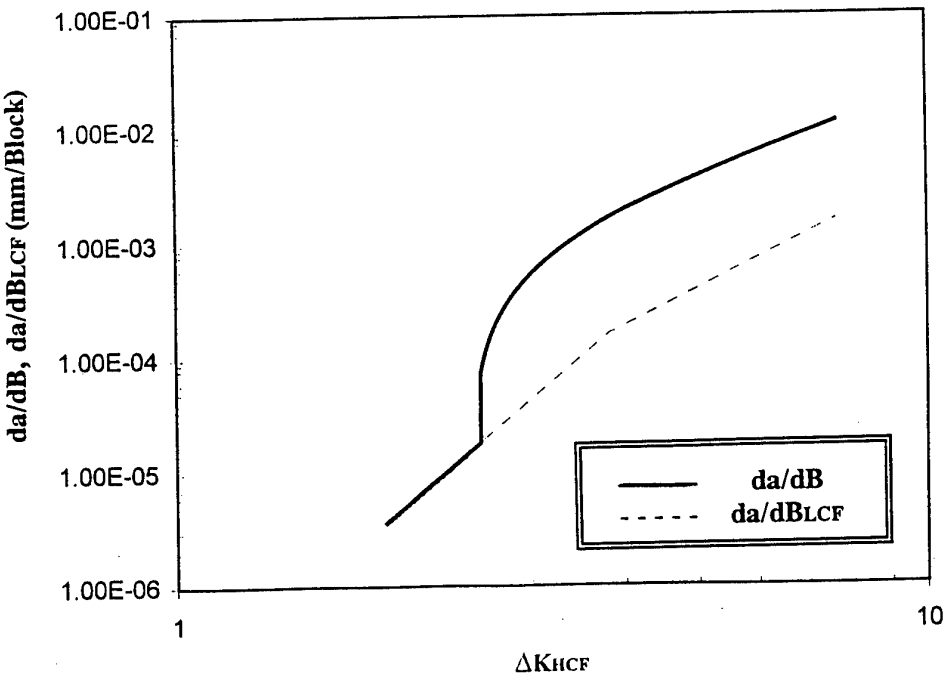

Figure 14(c) The effect of the number of HCF cycles - crack growth with a loading block of n = 10 000:1

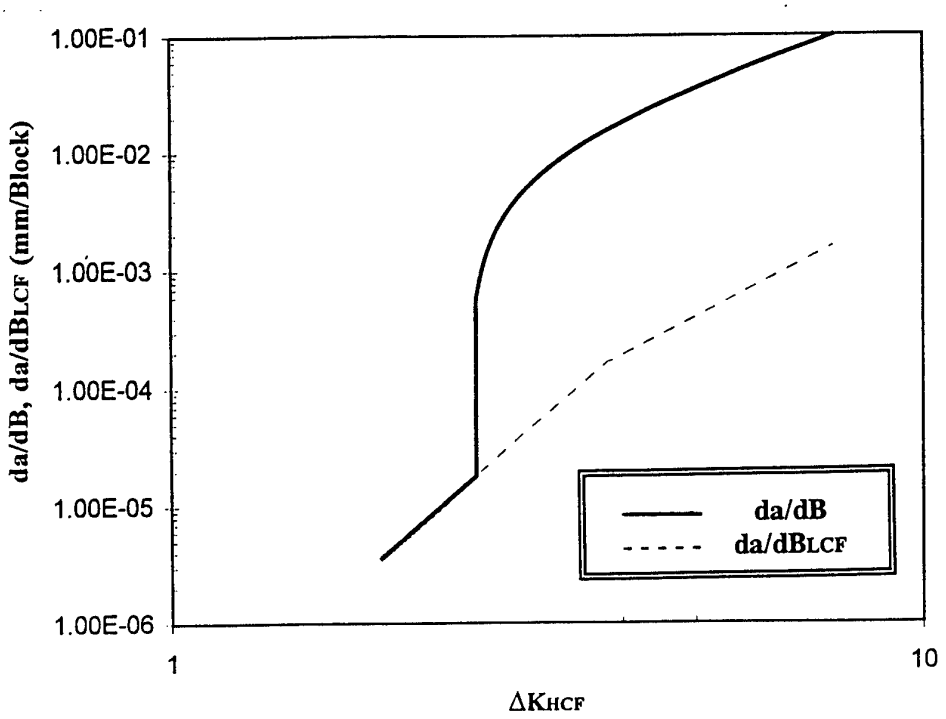

Figure 15(a) The effect of the number of LCF cycles - crack growth with a loading block of n = 1000:1

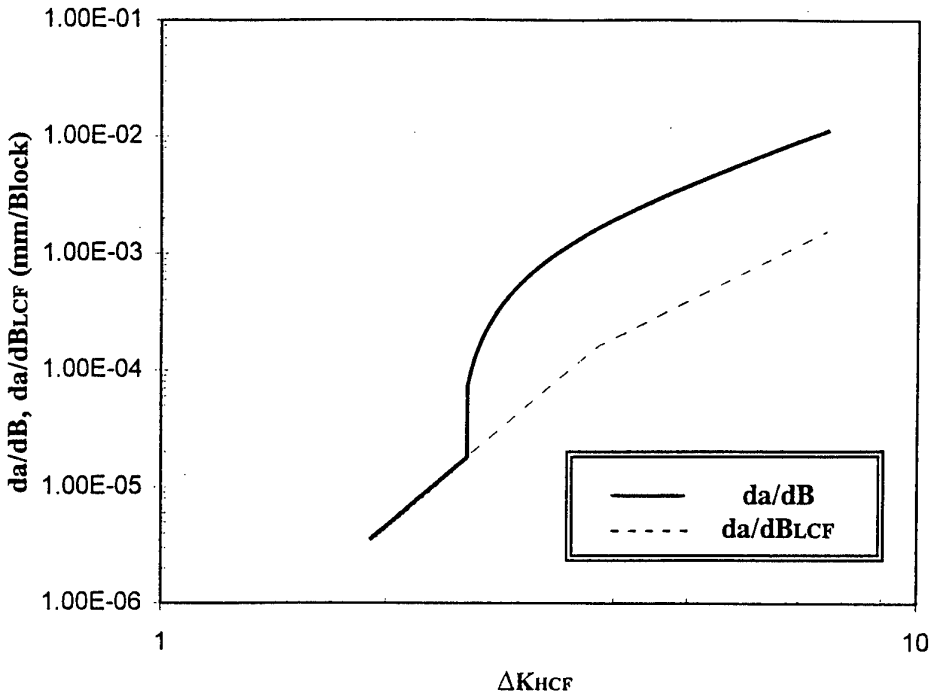

Figure 15(b) The effect of the number of LCF cycles - crack growth with a loading block of n = 1000:10

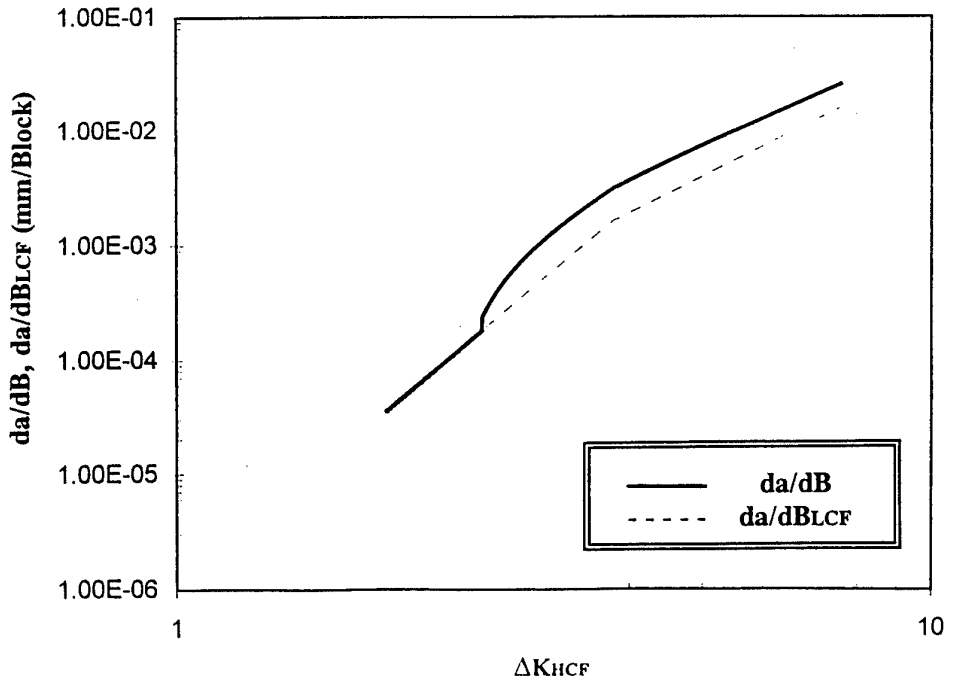

Figure 15(c) The effect of the number of LCF cycles - crack growth with a loading block of n = 1000:100

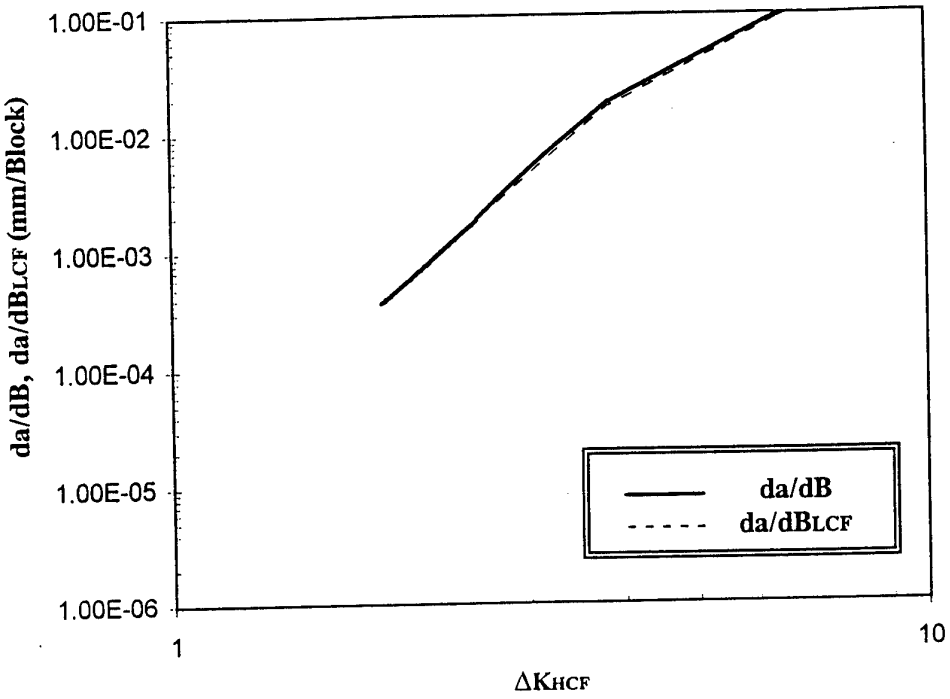

Figure 16(a) The effect of the number of LCF cycles - crack growth with a loading block of n = 10 000:1

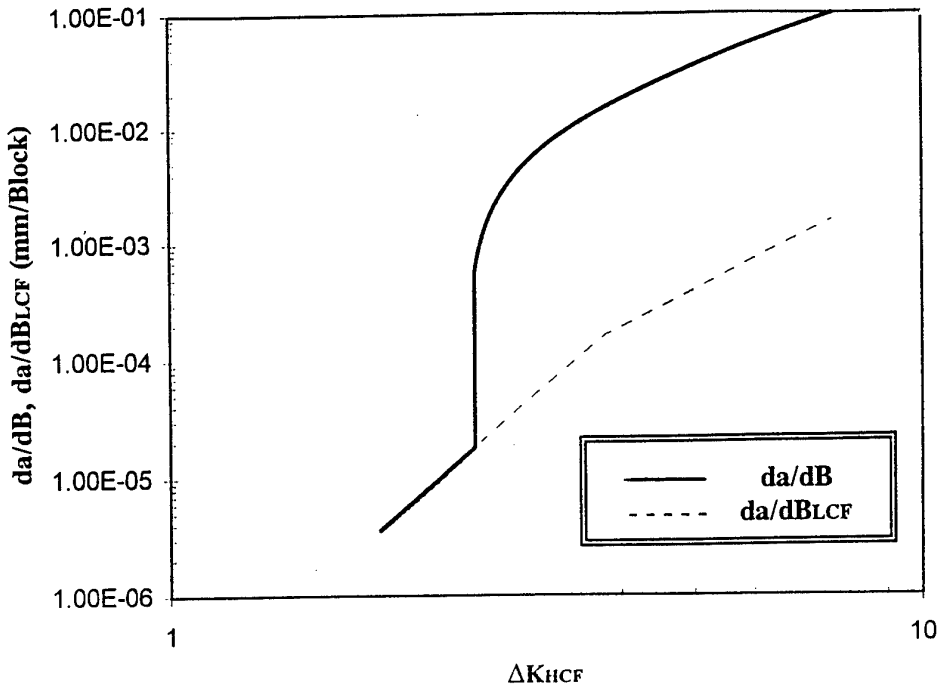

Figure 16(b) The effect of the number of LCF cycles - crack growth with a loading block of n = 10 000:10

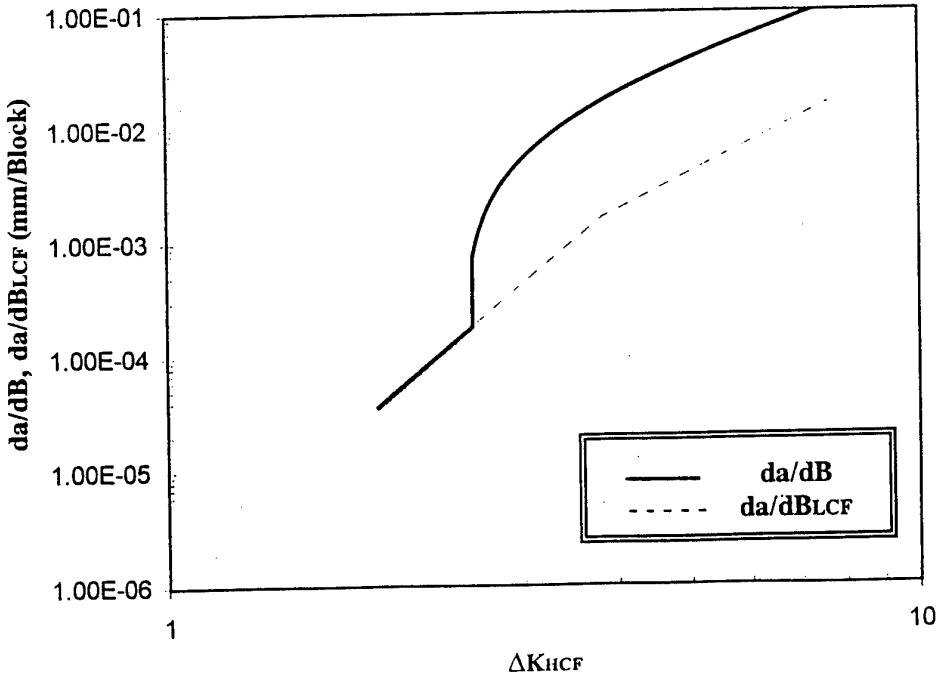

Figure 16(c) The effect of the number of LCF cycles - crack growth with a loading block of n = 10 000:100

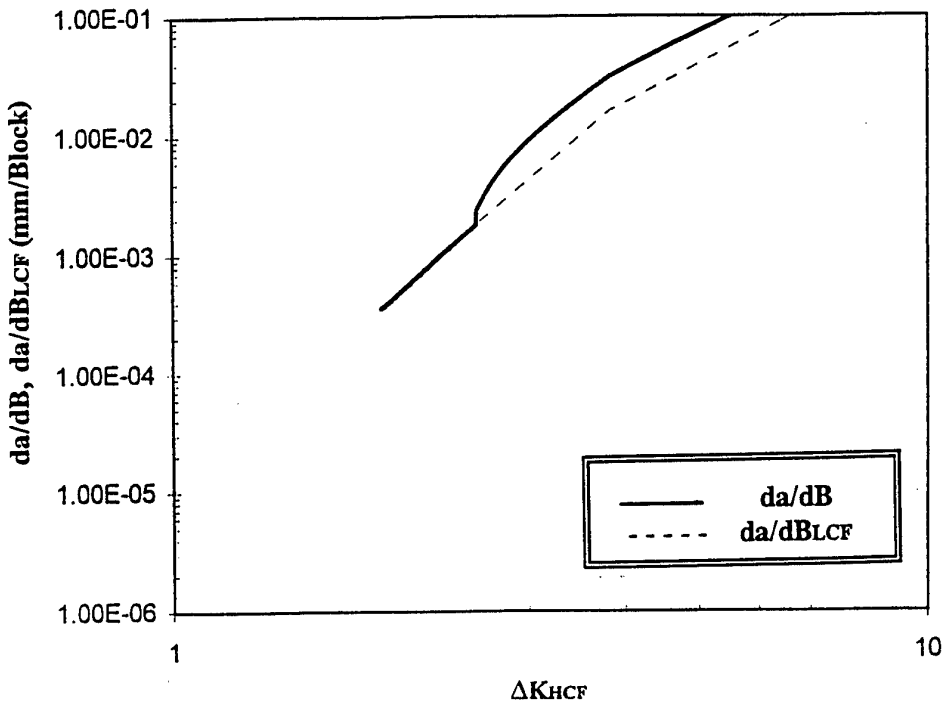

Figure 16(d) The effect of the number of LCF cycles - crack growth with a loading block of n = 10 000:1000

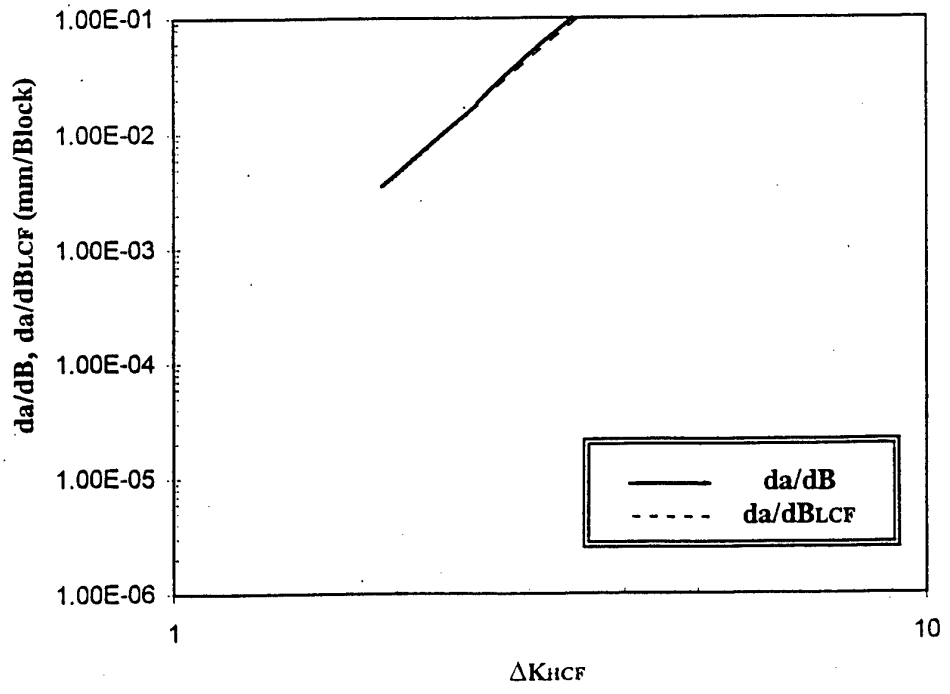

Figure 17(a) The effect of Wheeler's constant - crack growth with w = 1 and a loading block of n = 1000:1

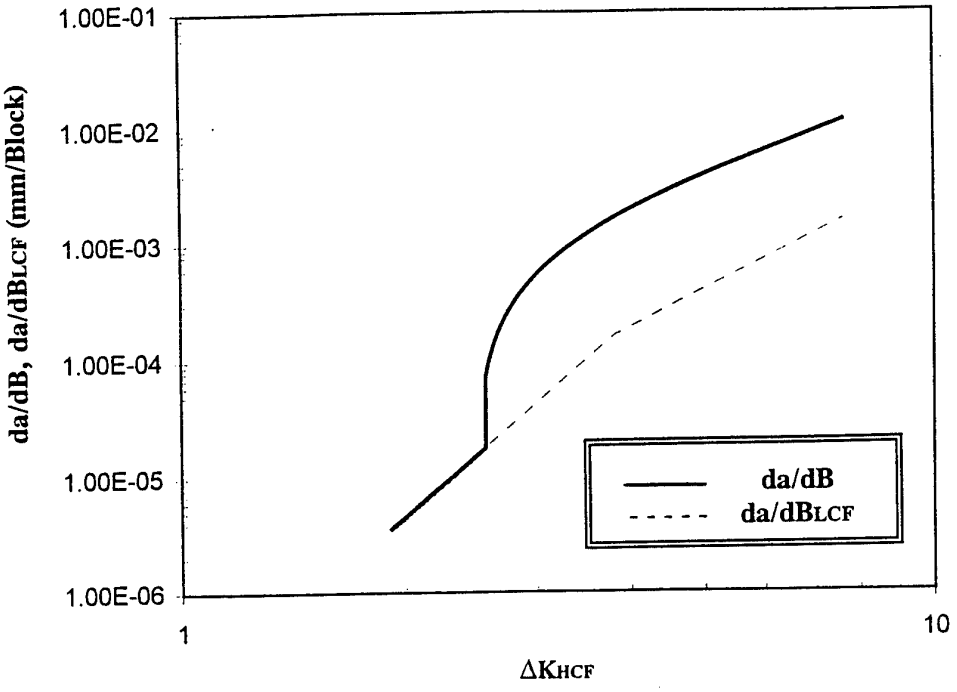

Figure 17(b) The effect of Wheeler's constant - crack growth with w = 6 and a loading block of n = 1000:1

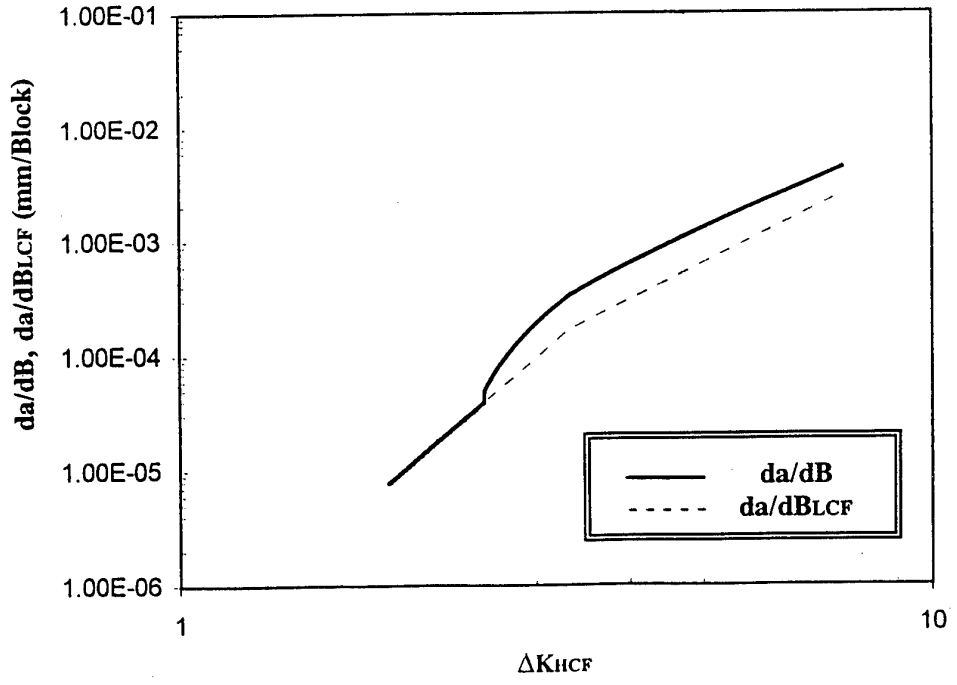

Figure 17(c) The effect of Wheeler's constant - crack growth with w = 12 and a loading block of n = 1000:1

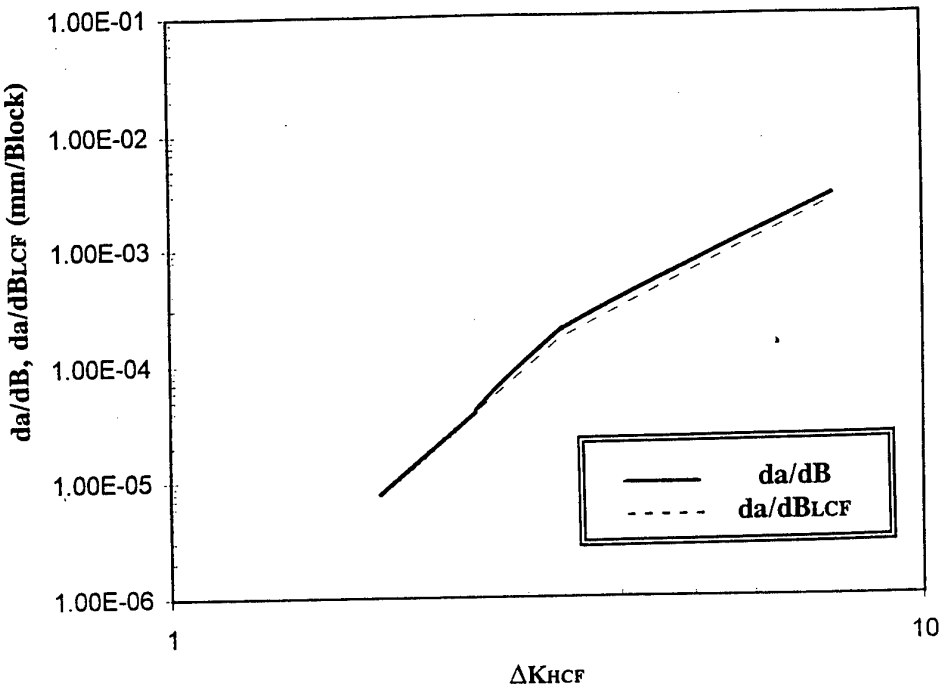

Figure 18(a) The effect of Wheeler's constant - crack growth with w = 1 and a loading block of n = 10 000:1

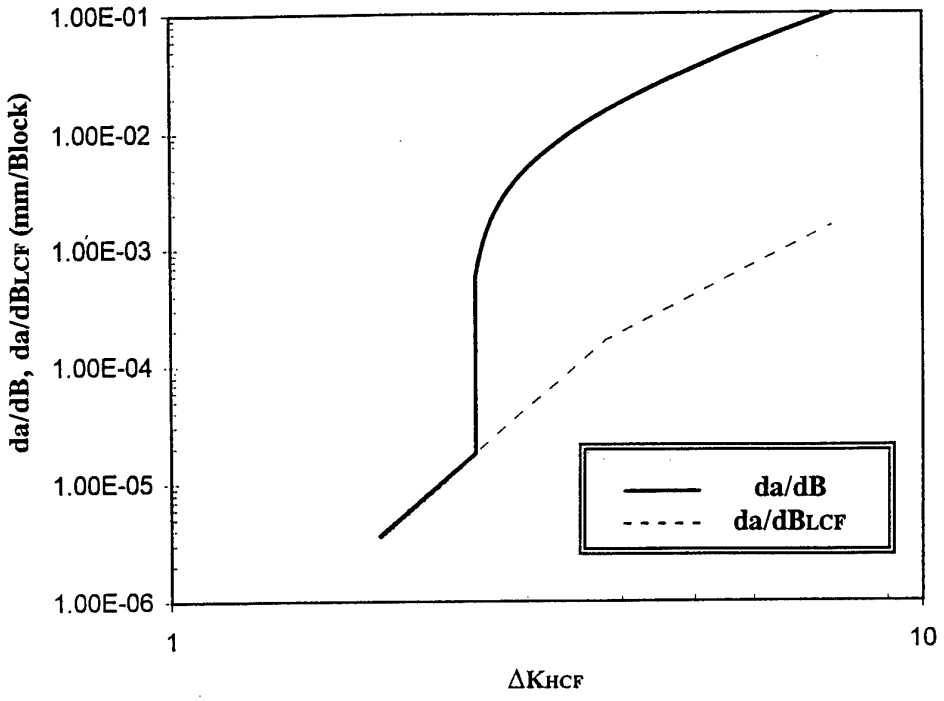

Figure 18(b) The effect of Wheeler's constant - crack growth with w = 6 and a loading block of n = 10 000:1

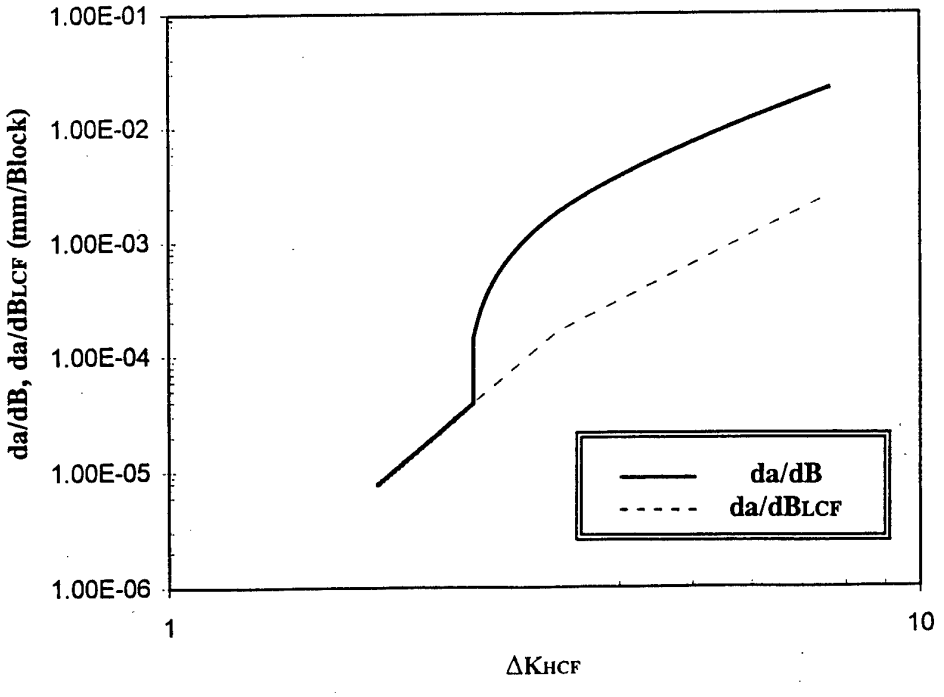

Figure 18(c) The effect of Wheeler's constant - crack growth with w = 12 and a loading block of n = 10 000:1

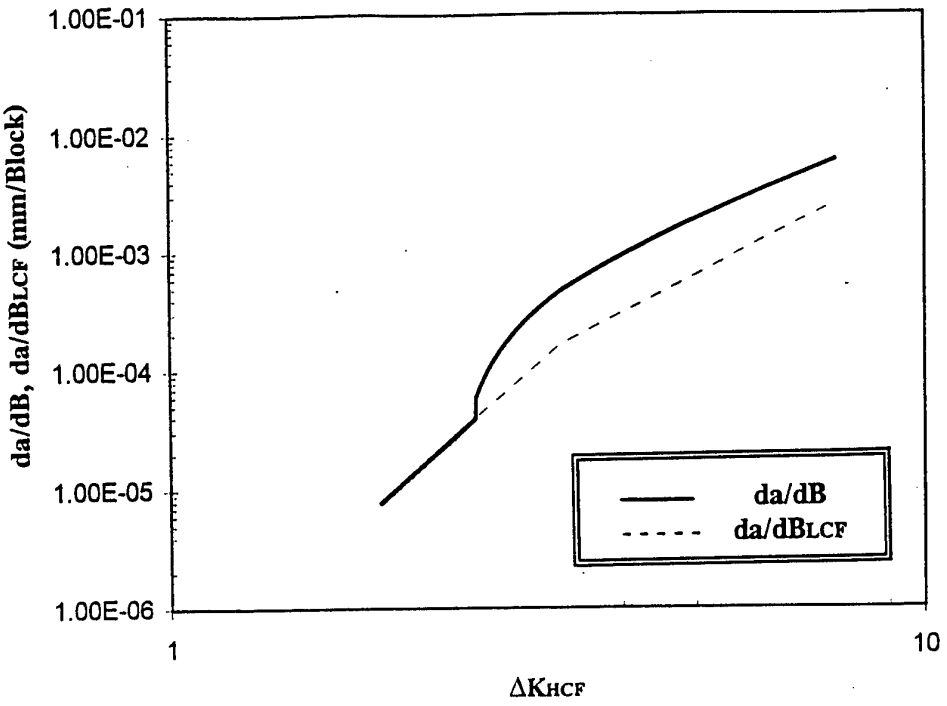

Figure 19(a) The effect of the number of LCF overload cycles - crack growth with w = 6 and a loading block of n = 1000:1

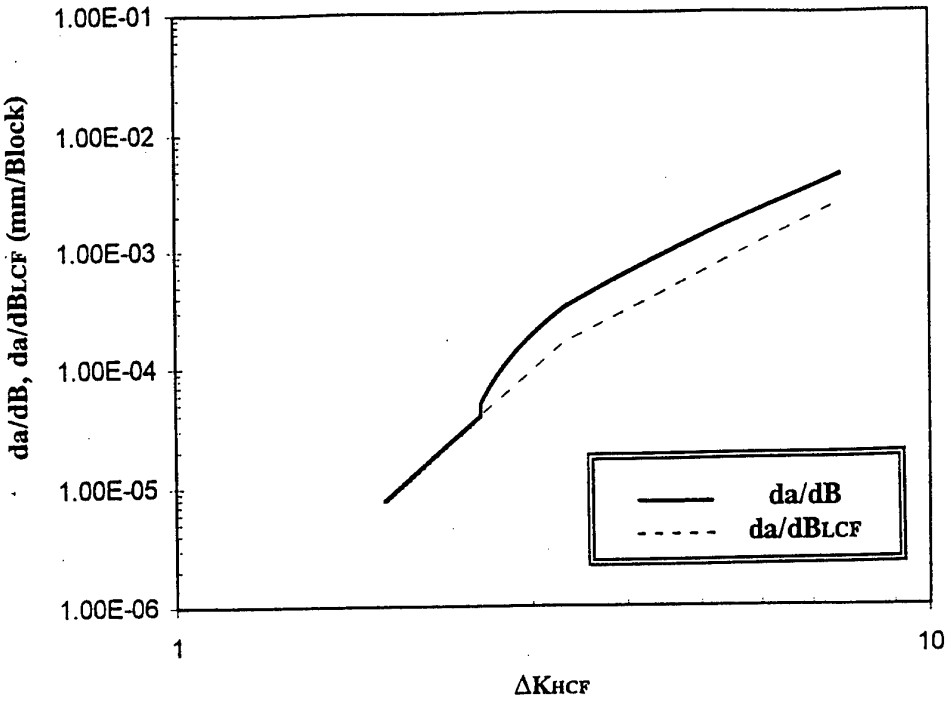

Figure 19(b) The effect of the number of LCF overload cycles - crack growth with w = 6 and a loading block of n = 1000:10